HHS Public Access

Author manuscript

Acta Biomater. Author manuscript; available in PMC 2017 October 01.

Published in final edited form as:

Acta Biomater. 2016 October 01; 43: 122–138. doi:10.1016/j.actbio.2016.07.043.

Combination scaffolds of salmon fibrin, hyaluronic acid, and laminin for human neural stem cell and vascular tissue engineering

Janahan Arulmoli[a,b], **Heather J. Wright**[b,c], **Duc T.T. Phan**[c], **Urmi Sheth**[b], **Richard A. Que**[a], **Giovanni A. Botten**[d], **Mark Keating**[a], **Elliot L. Botvinick**[a,h], **Medha M. Pathak**[b,e], **Thomas I. Zarembinski**[f], **Daniel S. Yanni**[g], **Olga V. Razorenova**[b,c], **Christopher C.W. Hughes**[a,c,h], and **Lisa A. Flanagan**[a,b,i,*]

[a]Department of Biomedical Engineering, University of California, Irvine, Irvine, CA 92697, USA

[b]Sue & Bill Gross Stem Cell Research Center, University of California, Irvine, Irvine, CA 92697, USA

[c]Department of Molecular Biology and Biochemistry, University of California, Irvine, Irvine, CA 92697, USA

[d]Department of Microbiology, Immunology & Molecular Genetics, University of California, Los Angeles, Los Angeles, CA 90095, USA

[e]Department of Physiology & Biophysics, University of California, Irvine, Irvine, CA 92697, USA

[f]BioTime, Inc., 1301 Harbor Parkway, Alameda, CA 94502, USA

[g]Disc Comfort, Inc., 351 Hospital Road, Suite 202, Newport Beach, CA 92663, USA

[h]The Edwards Lifesciences Center for Advanced Cardiovascular Technology, University of California, Irvine, Irvine, CA 92697, USA

[i]Department of Neurology, University of California, Irvine, Irvine, CA 92697, USA

Abstract

Human neural stem/progenitor cells (hNSPCs) are good candidates for treating central nervous system (CNS) trauma since they secrete beneficial trophic factors and differentiate into mature CNS cells; however, many cells die after transplantation. This cell death can be ameliorated by inclusion of a biomaterial scaffold, making identification of optimal scaffolds for hNSPCs a critical research focus. We investigated the properties of fibrin-based scaffolds and their effects on hNSPCs and found that fibrin generated from salmon fibrinogen and thrombin stimulates greater hNSPC proliferation than mammalian fibrin. Fibrin scaffolds degrade over the course of a few days *in vivo*, so we sought to develop a novel scaffold that would retain the beneficial properties of fibrin but degrade more slowly to provide longer support for hNSPCs. We found combination scaffolds of salmon fibrin with interpenetrating networks (IPNs) of hyaluronic acid (HA) with and

*Corresponding author at: Department of Neurology, University of California, Irvine, 3030 Gross Hall, 845 Health Sciences Rd., Irvine, CA, 92697-1705, USA. lisa.flanagan@uci.edu (L.A. Flanagan).

without laminin polymerize more effectively than fibrin alone and generate compliant hydrogels matching the physical properties of brain tissue. Furthermore, combination scaffolds support hNSPC proliferation and differentiation while significantly attenuating the cell-mediated degradation seen with fibrin alone. HNSPCs express two fibrinogen-binding integrins, αVβ1 and α5β1, and several laminin binding integrins (α7β1, α6β1, α3β1) that can mediate interaction with the scaffold. Lastly, to test the ability of scaffolds to support vascularization, we analyzed human cord blood-derived endothelial cells alone and in co-culture with hNSPCs and found enhanced vessel formation and complexity in co-cultures within combination scaffolds. Overall, combination scaffolds of fibrin, HA, and laminin are excellent biomaterials for hNSPCs.

Keywords

Neural stem cell; Biomaterial scaffold; Hydrogel; Neural tissue engineering; Integrin; Co-culture; Salmon fibrin; Hyaluronic acid; Laminin; Neurovascular niche; Matrix mechanics

1. Introduction

Stem cells are an important component of tissue engineering and regenerative medicine approaches since they provide beneficial secreted molecules to stimulate repair and can replace lost cells [1]. CNS neural stem cells are multipotent stem cells capable of self-renewal and differentiation into more committed progenitors that can generate neurons, astrocytes, and oligodendrocytes [2]. Transplanted neural stem and progenitor cells (NSPCs) migrate to areas of injury, actively respond to the microenvironment, secrete neuroprotective compounds, generate differentiated cells, and improve functional recovery [3–7]. However, a significant limitation of stem cell transplantation into the damaged CNS is that most cells die upon injection, with reports of surviving cells ranging from 0% to 30% at 4 weeks post-transplant for non-immortalized human NSPCs (hNSPCs) in rodent models of ischemic stroke [8]. The incorporation of NSPCs into a biocompatible scaffold, which is a 3-dimensional structure that supports tissue formation, can alleviate low cell survival post-transplant. For example, inclusion of a scaffold increases survival of NSPCs transplanted into rodent models of stroke [9] and traumatic brain injury (TBI) [10]. Scaffolds provide a 2-fold increase in mouse NSPC survival 2 weeks post-transplant into the infarct core of a mouse stroke model [9]. Furthermore, scaffolds increase survival of mouse NSPCs in a mouse model of TBI up to 5.6-fold at 8 weeks post-transplant and induce significant improvements in cognitive function [10]. Thus identifying beneficial scaffolds for hNSPCs is critical for realizing their therapeutic potential.

Three-dimensional scaffolds provide stem cells with an appropriate microenvironment and recapitulate the functions of native tissue [11–13]. Thorough scaffold characterization in an *in vitro* setting is essential for optimizing key parameters that support NSPC function. This must be done prior to implementation in animal models of injury in which the *in vivo* niche is quite complex. Critical scaffold attributes for NSPC transplantation into CNS tissue [14] include non-toxic polymerization, biocompatibility with both transplanted NSPCs and host tissue, the ability to be injected as a liquid and polymerize *in situ* to form a tight apposition with the host tissue, and mechanical properties that match that of the CNS. The scaffold

must also support vascularization to provide nutrient delivery to cells within the scaffold, have non-toxic degradation by-products and a degradation rate that allows sufficient time for cellular integration. Extracellular matrix (ECM) components such as proteins and polysaccharides are attractive candidates for scaffolds since they are biocompatible, contain sites for cellular adhesion, and provide suitable substrates for stem cell survival, growth, and function.

Fibrin is an ECM protein involved in blood clotting during the coagulation cascade and is non-toxic and biocompatible. Fibrin hydrogels are formed when fibrinogen is cleaved by thrombin to generate fibrin monomers that are covalently crosslinked by Factor XIIIa to create a mesh, which can be degraded by the enzyme plasmin. By varying the concentrations of fibrinogen and thrombin, the mechanical properties and polymerization time of the hydrogel can be modulated [15]. Fibrin contains multiple adhesive sites including RGD sequences that engage integrins on the cell surface. Fibrin has been used as a scaffold for mouse and human NSPCs and as a growth factor delivery vehicle in rodent spinal cord injury models [16–19]. Intriguingly, the source of fibrin can play an integral role in its effectiveness as a scaffold. Salmon fibrin, as opposed to human and bovine fibrin, encourages greater neurite outgrowth of rodent CNS neurons and better resists degradation by cellular proteases [20,21]. Salmon fibrin matches the mechanical characteristics of CNS tissue [20,22] and when used to treat rats with dorsal hemisection spinal cord injuries promotes greater locomotor functional recovery, density of serotonergic fibers caudal to the lesion site, and recovery of bladder function than mammalian fibrin [23]. Salmon fibrin has been developed as a human therapeutic and has passed numerous toxicity and immunogenicity tests [24,25]. Although salmon fibrin is an effective scaffold to treat CNS injury [23], it degrades rapidly *in vivo* (~7 days) and thus is unlikely to provide long-term support for transplanted hNSPCs.

In order to mitigate this rapid degradation, we designed combination scaffolds of fibrin and a material commonly found in the NSPC niche within the brain, hyaluronic acid (HA) [26], which has been shown to persist for at least 2 months when transplanted into the CNS [27,28]. HA is a naturally occurring polysaccharide present in the ECM that is high in the developing brain and in the postnatal brain in regions adjacent to the lateral ventricles where stem cells reside [26,29]. HA has been developed as a biomaterial for NSPC applications [30] including tissue repair after acute ischemic stroke [27,28]. HA scaffolds increase the survival of transplanted mouse NSPCs twofold, promote the differentiation of human induced pluripotent stem cell (iPS)-derived NSPCs into immature neurons, and reduce the host inflammatory response when transplanted into the infarct stroke cavity of a mouse model [9,31]. HA has advantages as a scaffold material but is not always sufficient to promote cell adhesion [32,33], so can be combined with adhesive peptides or another ECM component to provide cell attachment. Thus, combination scaffolds of fibrin and HA may benefit from the cell adhesive properties of fibrin and degradation rate of HA.

Another ECM component beneficial for neural cells that can be incorporated into scaffolds is laminin. Laminin stimulates hNSPC expansion, migration, and differentiation [34] and can be used to functionalize various biomaterials to encourage neural cell adhesion in neural tissue engineering applications [35,36]. Laminin-containing collagen-based scaffolds

significantly improve the survival of mouse NSPCs 8 weeks after transplant into the traumatically injured mouse brain and animals treated with laminin-containing scaffolds and NSPCs perform better in behavioral tests than untreated controls [10]. Matrigel scaffolds, which are predominantly collagen and laminin, seeded with embryonic stem cell-derived hNSPCs decrease infarct volume after focal cerebral ischemia in rats compared to cell transplants alone [37]. HA-laminin scaffolds enhance NSPC migration in response to stromal cell-derived factor-1α (SDF-1α) gradients, which arise from injured brain tissue [38]. Interestingly, HA in the scaffolds leads to upregulation of the SDF-1α receptor, CXCR4, on NSPCs while enhanced migration is dependent on both HA and laminin in the scaffolds. Since laminin has beneficial effects on NSPCs and hNSPCs express laminin-binding integrins [34,39], we tested laminin in our combination scaffolds with fibrin and HA.

The biomaterial composition of the scaffold affects its vascularization *in vivo*, which is critical for bringing nutrients to transplanted cells. Crosstalk between endothelial cells and NSPCs also impacts NSPC function and has inspired interest in the *in vivo* neurovascular niche. Endothelial cells promote proliferation and neuronal differentiation of rodent NSPCs in culture and slice models, mediated at least in part through VEGF produced by endothelial cells acting on NSPC VEGF receptors and upregulation of genes in the Notch pathway in NSPCs [40–43]. NSPCs and endothelial cells/vessels are closely associated *in vivo*, creating neurovascular niches that can be mimicked by including both cell types in scaffold constructs [44]. Co-transplantation of mouse NSPCs and either mouse or bovine endothelial cells without a scaffold into rodent stroke models leads to greater numbers of integrated NSPCs, greater NSPC proliferation, more neuronal differentiation, and improved functional recovery [45,46]. A poly (ethylene glycol)-based scaffold containing mouse NSPCs and mouse endothelial cells transplanted subcutaneously formed better vessels than transplants of endothelial cells alone in the scaffold [47]. In order to test scaffold and NSPC effects on vasculogenesis and to incorporate components of the human neurovascular niche, we added human endothelial colony-forming cell-derived endothelial cells (hECFC-ECs) to the scaffolds. Determining optimal scaffold and cell conditions to encourage vascularization *in vitro* may accelerate the formation of functional vasculature after transplantation [48–50].

While fibrin and HA have been tested individually as scaffolds, they each have limitations that may be overcome by incorporating them into a combination scaffold. The goal of our study was to compare fibrin and combination scaffolds to determine their material properties, effects on hNSPCs, and potential for vascularization. The polymerization kinetics and mechanical properties of the scaffolds were tested to determine whether they could be used as injectable scaffolds and match the stiffness of CNS tissue. HNSPCs were seeded in scaffolds to test cell proliferation and differentiation and hNSPC cell surface integrins for scaffold binding were identified. Since degradation of fibrin only scaffolds occurred rapidly *in vivo* [23], the degradation of fibrin and combination scaffolds seeded with hNSPCs was assessed over time and at multiple cell concentrations. Co-cultures of hNSPCs and hECFC-ECs in the scaffolds were utilized to measure vasculogenesis as a function of scaffold biomaterial and cellular composition and to assess potential for vascularization. These studies enabled crosstalk between vascular endothelial cells and neural cells, creating a neurovascular niche that affects NSPC function [42,44,51] as well as endothelial cell

behavior and vasculogenesis [47,52,53]. A comparison of fibrin only and combination scaffolds across multiple parameters allowed a thorough analysis of their potential use as scaffolds for hNSPCs.

2. Materials & methods

2.1. Cell culture

Fetal-derived hNSPCs (SC27 and SC23) were isolated from the cerebral cortices of two separate brains by the National Human Neural Stem Cell Resource and were grown as adherent cultures on 6-well plates coated with 10 μg/mL fibronectin (human; Fisher Scientific, Hampton, NH, USA) [54]. HNSPC basal medium included DMEM/F12 (Fisher Scientific, Hampton, NH, USA), 20% BIT 9500 (bovine serum albumin, insulin, and transferrin; Stem Cell Technologies, Vancouver, CA), and 1% antibiotic/antimycotic (penicil lin/streptomycin/amphotericin; Thermo Fisher Scientific, Waltham, MA, USA). Proliferation media was prepared from basal media via addition of 40 ng/mL epidermal growth factor (EGF; PeproTech, Rocky Hill, NJ, USA), 40 ng/mL basic-fibroblast growth factor (bFGF; PeproTech), and 20 ng/mL platelet-derived growth factor (PDGF-AB; PeproTech,). Proliferation was measured at 3, 6, or 7 days post cell-seeding in proliferation media. Astrocyte differentiation media consisted of DMEM/F12, 20% fetal bovine serum (FBS; Gibco, Waltham, MA, USA), and 1% antibiotic/antimycotic. Neuronal differentiation media consisted of 96% Neurobasal (Thermo Fisher Scientific, Waltham, MA, USA), 2% B-27 (Thermo Fisher Scientific), 1% GlutaMAX (Thermo Fisher Scientific), and 1% pen/strep (penicillin/streptomycin; Thermo Fisher Scientific) with 20 ng/mL brain-derived neurotrophic factor (BDNF; PeproTech), 20 ng/mL glial-derived neurotrophic factor (GDNF; PeproTech), and 0.5 μM dibutyryl cyclic AMP (cAMP; Sigma-Aldrich, St. Louis, MO, USA) (modified from [55]). HNSPCs were differentiated for 5 days in astrocyte differentiation media and 14 days in neuronal differentiation media. Cells were routinely passaged 1:2 or 1:3 and seeded at 5×10^4–1×10^6 hNSPCs per 100 μL hydrogel for experiments and equal numbers of viable cells (Trypan Blue staining) were used for each experimental group. Proliferation media was refreshed every day (50%) for passaging and every other day (100%) for scaffold proliferation assays to minimize mechanical disruption of the gels with daily media changes. Differentiation media was refreshed (100%) every other day. For co-culture experiments, hNSPCs were tagged with CellTracker Green (Thermo Fisher Scientific; C2925) at 10 μM for 45 min prior to seeding into scaffolds.

HECFC-ECs were isolated from cord blood as previously described with approval from UC Irvine's Institutional Review Board [56]. After isolation, cells were expanded on flasks coated with 10 μg/mL fibronectin (human; Fisher Scientific) in EGM-2 media supplemented with a growth factor bullet kit (Lonza, Basel, SUI; CC-3162). HECFC-EC were transduced with lentivirus to express mCherry fluorescence. Lentiviral constructs (LeGO-C2) were gifts from Boris Fehse (Addgene plasmids, Cambridge, MA, USA; 27339). Cells were used for experiments between passages 4 and 8. All cell types were cultured in a 37 °C, 5% CO_2 humidified incubator.

2.2. Hydrogel/scaffold formulation

Fibrin gels were formulated by cleaving 5 mg/mL salmon fibrinogen (SeaRun Holdings, Inc.) with 2 U/mL salmon thrombin (SeaRun Holdings, Inc.) in Minimal Essential Media (MEM; Thermo Fisher Scientific). For combination hydrogels, 1 mg/mL thiolated Hyaluronic Acid (HA) (Glycosil®; BioTime, Inc.) (average molecular weight (MW) ~250 kDa) with or without 100 μg/mL laminin (Thermo Fisher Scientific) was included in the hydrogel mixture prior to addition of thrombin. HA of 250 kDa MW was chosen for these studies since HA of this size has a lower viscosity and is readily modified in a reaction vessel via thiol addition to carboxylic acid groups on the repeating HA disaccharide chain [57,58]. This thiol modification allows for the straightforward addition of cell adhesion peptides or cross-linking sites to the HA hydrogel. The MW of this HA is within the range of sizes of HA used successfully as scaffolds for transplantation (60 kDa–1.6 MDa) [28,31,59] and 250 kDa HA increases survival of transplanted NSPCs [9,60]. Bovine and human fibrinogen and thrombin were obtained from Calbiochem or Sigma as lyophilized proteins and had endotoxin levels less than 0.5 EU/mL. HNSPC and/or hECFC-EC cell solution was added at a volume of 50 μL and mixed with 50 μL of hydrogel solution to create 100 μL scaffolds, cultured on 18 mm diameter cover slips in 12-well plates.

2.3. Cell proliferation assay

The Click-iT EdU kit (Thermo Fisher Scientific) was used to identify hNSPCs entering S-phase of the cell cycle. HNSPCs were seeded at 1×10^5 cells per 100 μL hydrogel and cultured in proliferation medium supplemented with 10 μM EdU nucleoside analog at 37 °C for 6 h. The scaffold constructs were fixed, permeabilized, and blocked as previously described [34]. A copper ion (Cu^{1+}) catalyzes a covalent bond between an Alexa Fluor azide and an alkyne in the EdU in the Click-iT reaction. All cell nuclei were stained with 4 μg/mL Hoechst 33342 in PBS. The percentage of EdU-positive cells was determined by quantifying 3–5 randomly selected fields from each scaffold group imaged using a Zeiss Spinning Disc Confocal Microscope (Zeiss, Oberkochen, DEU).

2.4. Scaffold degradation and assessment of soluble fibrinogen

Fibrin scaffold degradation and amount of soluble fibrinogen in the media was determined using Western Blot. Briefly, 1×10^5, 3×10^5, 6×10^5, 1×10^6, or no cells were seeded in fibrin only, fibrin/HA, or fibrin/HA/laminin scaffolds. Proliferation media was added 30 min after initial polymerization was induced with thrombin. In order to assess the amount of soluble fibrinogen released from hydrogels not seeded with cells, media samples for Western Blot were taken immediately after adding media to polymerized hydrogels lacking cells. These were used as control samples to determine fold changes in degradation in comparison to cell-seeded hydrogels. After 7 or 30 days in culture in a 37 °C, 5% CO_2 humidified incubator, 1–5 μL of conditioned media was removed from the well and mixed with SDS loading buffer (312 mM Tris HCl pH 6.8, 10% SDS, 0.05% bromophenol blue, 50% glycerol, 10% beta-mercapto ethanol). Samples were loaded in each lane of 10% bis-acrylamide gels and transferred onto 0.2 μm nitrocellulose membranes (BioRad). Within a single experiment, an equal amount of media was withdrawn from each sample for analysis. Blots were stained with Ponceau S to detect total protein. Ponceau S staining and mouse

anti-transferrin were used to verify equal loading and transfer of each lane since transferrin is a component of the cell culture media. The primary antibodies used were 1:50,000 dilution of rabbit anti-salmon fibrinogen [23] and 1:1000 dilution of mouse anti-transferrin (Abcam, Cambridge, UK; ab10208). Membranes were incubated with primary antibodies overnight at 4 °C with gentle agitation. The following secondary antibodies were used: goat anti-mouse HRP conjugate (Thermo Fisher Scientific; # 31430), goat anti-rabbit HRP conjugate (Pierce #31460), horse anti-mouse AP (Vector Labs, Burlingame, CA, USA; #AP-2000). Membranes were incubated with secondary antibodies for 1 h at room temperature with gentle agitation and the signal was developed using Amersham ECL Prime western blotting substrate (GE Healthcare, Scottsdale, AZ, #RPN2236) or SigmaFast BCIP/NBT substrate (Sigma Aldrich; #B5655) for HRP or AP conjugates, respectively. Standard curves were generated by loading a range of 1–1000 ng of salmon fibrinogen for every experiment to accurately assess linearity of protein detection and degradation within experimental groups. ImageJ software was used to obtain quantitative measurements of band intensity for comparison between groups through the integrated density function, which sums the values of the pixels for a given band. The integrated density values for the bands in the standard curve for each experiment was used to correlate the specific amount of fibrinogen released in the experimental groups. It should be noted that fold change in fibrinogen detection across conditions was used for some analyses rather than total amount (μg) in order to control for minor variations in scaffold degradation across experiments.

2.5. Mechanical characterization of hydrogels

Bulk rheology was used to obtain the viscoelastic properties of the hydrogels. Elastic and viscous moduli were quantified using a stress-controlled rheometer (Anton Paar; MCR 301, Graz, Austria) with a 25 mm diameter parallel plate geometry. Samples containing salmon fibrinogen (5 mg/mL) alone or with HA (1 mg/mL) were diluted in MEM and mixed with salmon thrombin (2 U/mL). The hydrogels were prepared at a total volume of 140 μL and immediately loaded onto the rheometer upon addition of thrombin. A humidified chamber was created via a solvent trap filled with deionized H_2O in order to prevent hydrogel evaporation during analysis. Oscillatory measurements were taken at a frequency of f = 1 Hz and strain of γ = 1% with a height gap of 200 μm. A Peltier temperature control system kept the chamber at 22.5 °C. The elastic (G') and viscous (G'') moduli were recorded over a time sweep until there was no longer a change in G'. The time sweep was subsequently followed by a frequency sweep performed at γ = 1% from f = 0.01 to 100 Hz. At the conclusion of the frequency sweep, a strain sweep was successively performed at f = 1 Hz from γ = 1 to 10,000%.

Gel point of the hydrogels was analyzed by reducing the concentration of thrombin in the hydrogels to 0.15 U/mL in order to capture polymerization kinetics. Samples were prepared as described above and oscillatory measurements were performed at f = 1 Hz and γ = 1%. Measurements were obtained every 1 s in order to capture the time required to transition from liquid to viscoelastic solid ($G' = G''$).

2.6. Immunostaining and imaging

For the purposes of immunocytochemistry, scaffold constructs were fixed with 4% paraformaldehyde for 20 min. After 4×15 min PBS washes, cells were treated with 0.3% Triton X-100 (Sigma) in PBS for 15 min followed by 4×15 min PBS washes. Constructs were then blocked using 10% donkey serum, 5% BSA, 0.1% Triton X-100 in PBS overnight at 4 °C on a rocker. Primary antibodies were diluted in 10% donkey serum, 5% BSA, 0.1% Triton X-100 in PBS and were incubated overnight at 4 °C on a rocker. The following primary antibodies were used: rabbit anti-Ki67 (Leica Biosystems, Wetzlar, DEU; KI67P-CE) diluted 1:500, mouse anti-GFAP (Sigma Aldrich; G3893) diluted 1:200, mouse anti-MAP2 (Sigma Aldrich; M4403) diluted 1:200, goat anti-doublecortin (Santa Cruz Biotechnology, Dallas, TX, USA; SC-8066 (c-18)) diluted 1:200. Following primary antibody incubation, scaffold constructs underwent 4×15 min PBS washes. Secondary antibodies were diluted in 10% donkey serum, 5% BSA, 0.1% Triton X-100 in PBS and were incubated with cells for 2 h in the dark at room temperature on a rocker. The following secondary antibodies were used at 1:200 dilutions: donkey anti-rabbit 555 (Thermo Fisher Scientific; A-31572), donkey anti-mouse 555 (Thermo Fisher Scientific; A-31570), donkey anti-goat 488 (Thermo Fisher Scientific; A-11055). Secondary antibody incubation was followed by 4×15 min PBS washes. Cell nuclei were counterstained with 4 μg/mL Hoechst 3342 in PBS for 5 min, followed by 1×15 min PBS wash. Scaffolds were mounted with 20 μL Vectashield (Vector Labs; H-1000) onto cover glass and imaged using a Zeiss Spinning Disc Confocal Microscope (Zeiss) using a 20× or 40× objective with numerical apertures 0.8 and 0.75, respectively. Images were acquired using AxioVision Rel 4.8 software. Each individual image stack was 80 μm thick using 1.3 μm slice thickness. ImageJ was used to quantitate positively stained cell nuclei for proliferation.

For confocal reflection microscopy, samples of the combination and fibrin scaffolds were prepared as described in Section 2.2 on 35 mm glass bottom dishes (MatTek) and then imaged using a reflection confocal system as previously used [61], with some modifications, to image the 3D architecture of non-labeled fibrin hydrogels [62]. Samples were imaged on an IX81 inverted microscope (Olympus) equipped with a FluoView 1200 laser scanning confocal unit (Olympus) using a 60× oil objective (PlanApo TIRFM 1.45 NA, Olympus) and 488 nm laser (Olympus). For each sample (n = 3 per hydrogel), 7 μm z-stacks of each hydrogel were taken with a step size of 100 nm. Presented images were contrast enhanced for viewing purposes.

2.7. Flow cytometry

Samples from proliferating, confluent cultures were dissociated from the culture surface as previously described [54]. Briefly, hNSPCs were harvested as a single cell suspension with Cell Dissociation Buffer (Thermo Fisher Scientific), incubated and labeled with primary antibodies for 30 min in the dark, and analyzed on an LSR II Flow Cytometer (BD Biosciences, Franklin Lakes, NJ, USA) using a 488 nm laser. Primary antibodies used were: FITC-labeled anti-human CD51 (anti-αV integrin, Biolegend, San Diego, CA, USA; 327907) and isotype control FITC-labeled mouse IgG2a (Biolegend; 400209) at 1:100 dilution in 5% BSA. An unstained control was included alongside the stained samples and propidium iodide was used to discern live from dead cells. Up to 10,000 events were

collected and stored electronically on the BD FACSDIVA software. FLOWJO software was used to quantitate the percentage of hNSPCs expressing CD51.

2.8. Vascular analysis

Quantitative analysis of vascular formation was performed using AngioTool [63]. Images were taken with a 20× objective with numerical aperture 0.8 on a Zeiss Spinning Disc Confocal Microscope (Zeiss) on day 5 post-seeding and analyzed for vessel percentage area, total number of branch points, and total vessel length. Five randomly selected fields were obtained from each condition for analysis.

2.9. RNA sequencing

RNA was isolated from SC27 passage 12, 15, and 17 hNSPCs grown to confluency in single wells of 6 well plates ($1–2\times10^6$ cells) using the Bio-Rad RNA Isolation Kit (Genicity, Irvine, CA, USA; G00065). Genomic DNA contamination of all RNA samples was assessed by using qRT-PCR for human 18S and GAPDH with and without reverse transcriptase and found to be insignificant. cDNA for qRT-PCR was synthesized using M-MLV reverse transcriptase (Promega). qRT-PCR was performed using TaqMan primers on an Abi ViiA7 qPCR machine (Applied Biosystems, Foster City, CA, USA).

Total RNA was further monitored for quality control using the Agilent Bioanalyzer Nano RNA chip and Nanodrop absorbance ratios for 260/280 nm and 260/230 nm. RNA library preparation and sequencing was performed at the UCI Genomics Core. Library construction was performed according to the Illumina TruSeq mRNA stranded protocol. The input quantity for total RNA was 250 ng and mRNA was enriched using oligo dT magnetic beads. The enriched mRNA was chemically fragmented for five minutes. First strand synthesis used random primers and reverse transcriptase to make cDNA. After second strand synthesis, the double-stranded cDNA was cleaned using AMPure XP beads and the cDNA was end repaired and the 3° ends were adenylated. Illumina barcoded adapters were ligated on the ends and the adapter ligated fragments were enriched by nine cycles of PCR. The resulting libraries were validated by qPCR and sized by Agilent Bioanalyzer DNA high sensitivity chip. The concentrations for the libraries were normalized and the libraries were multiplexed together. The concentration for clustering on the flowcell was 12.5 pM. The multiplexed libraries were sequenced on one lane using single read 100 cycles chemistry for the HiSeq 2500. The version of HiSeq control software was HCS 2.2.58 with real time analysis software, RTA 1.18.64.

For sequence mapping and bioinformatic analysis, RNA-Seq data was processed as described previously [64]. All bioinformatics analyses were conducted using the Galaxy platform [65]. Reads were aligned to the human GRCh37/hg19 reference genome with the TopHat program [66] using most default parameters. Alignments were restricted to uniquely mapping reads with two possible mismatches permitted. RPKM (reads per kilobase pair per million mapped reads) were calculated as described [67] for hg19 RefSeq genes using the SeqMonk program (http://www.bioinformatics.babraham.ac.uk/projects/seqmonk/). MRNA RPKMs were derived by counting exonic reads and dividing by mRNA length. Since all samples were from a single cell type (hNSPCs), we designated RPKM value cutoffs of

above 10 (high), 1–10 (moderate), and below 1 (low) to denote expression levels of genes of interest. As validation, highly expressed transcripts such as beta-actin and GAPDH fall into the high category (beta-actin 2247.6 ± 255.6, GAPDH 886.3 ± 105.6), as does the FGFR1 (57.45 ± 4.6) known to function in NSPCs, while FGFR2 is in the moderate category (2.36 ± 0.7), and the muscle marker MyoD is in the low category (0.023 ± 0.003). Factors listed as being involved in angiogenesis were obtained from a commercial human angiogenesis PCR array (Qiagen, Hilden, DEU) and combined with factors previously identified by the Hughes Lab at UCI.

2.10. Statistical analysis

All statistical analyses utilized a one-way single factor ANOVA with Tukey post hoc tests for multiple comparisons.

3. Results

3.1. hNSPC proliferation in scaffolds is dependent on the species of fibrin

Tissue engineered scaffolds for transplantation of stem cells to aid CNS regeneration should inherently support stem cell survival and growth. We investigated whether fibrin source influences the proliferative capacity of cerebral cortical hNSPCs since fibrin source significantly affects the extension of neurites from mammalian neurons, with longer neurites formed in salmon fibrin than human or bovine fibrin [20].

After 6 days in culture, greater numbers of hNSPCs were present in salmon fibrin scaffolds than in bovine or human fibrin (Fig. 1a). Proliferation, quantified as the percentage of cells in S-phase of the cell cycle detected by EdU incorporation, was significantly greater for hNSPCs in salmon fibrin than cells in mammalian fibrin (Fig. 1b). A similar trend of more proliferating hNSPCs in salmon fibrin was detected by immunostaining for the proliferation marker phospho-histone H3, which labels mitotic cells in M-phase of the cell cycle (number of phospho-histone H3-positive cells per field: salmon fibrin 15.6 ± 1.7; bovine fibrin 6.8 ± 1.0; human fibrin 9.4 ± 2.1).

3.2. Inclusion of HA increases polymerization efficiency and stiffness of salmon fibrin scaffolds

Polymerization kinetics and mechanical strength of injectable scaffolds are essential components of biomaterial design that can determine the outcome of a cellular therapeutic [68]. Salmon fibrin as a scaffold biomaterial improves locomotor functional recovery, serotonergic innervation, and bladder recovery in spinal cord injured rats [23], but the scaffold degrades within 1 week, which would allow little time to support hNSPCs post-transplant. We thus created combination scaffolds of salmon fibrin and an interpenetrating network (IPN) of thiolated hyaluronic acid, which has been used previously as a scaffold for CNS transplantation [31,60], to test whether the combined biomaterial would have different degradation and mechanical properties than fibrin hydrogels. We incorporated laminin in combination scaffolds due to its prominent role as an ECM in the NSPC niche and because it stimulates hNSPC expansion, migration, and differentiation [34,69–71].

A conventional rheometer was used to characterize the polymerization time of the single and combination hydrogels. The polymerization time, or gel point, is defined here as the time required for the hydrogel's storage modulus (G') and loss modulus (G'') to be equal. The time sweeps for the hydrogels show that fibrin/HA reaches gel point significantly faster than fibrin alone (Fig. 2a,b). To analyze the extent of polymerization, the amount of non-polymerized fibrinogen associated with the different hydrogels was assessed by collecting media for Western Blot analysis of fibrinogen after hydrogel gelation. Initial experiments clarified linear detection of soluble fibrinogen using this approach (Fig. S1). After polymerization was complete, significantly more non-polymerized fibrinogen was released from fibrin hydrogels than hydrogels with HA included, while the presence of laminin in the hydrogels had no additional effect (Fig. 2c). While there is significantly less soluble fibrinogen remaining after polymerization of the combination hydrogels, the vast majority of the 500 μg fibrinogen in the polymerization reaction is incorporated into the hydrogels in all cases. Polymerization of combination hydrogels is more rapid and complete than fibrin hydrogels.

Since mechanical properties of the microenvironment affect stem cells [72,73], the mechanical properties of each hydrogel were measured using bulk rheology. The viscoelastic properties of fibrin and fibrin/HA scaffolds were independently characterized using conventional rheology, until G' and G'' remained relatively stable (Fig. 3a top). The hydrogels were initially more viscous at early time points near polymerization ($G'' > G'$), but demonstrated more elastic behavior as gelation progressed ($G' > G''$). Both G' and G'' remained relatively independent of frequency (Fig. 3a middle) and strain (Fig. 3a bottom), which are hallmark characteristics of viscoelastic materials [74,75]. Hydrogels with HA were significantly stiffer than those of fibrin alone, but both hydrogels were less than 250 Pa (fibrin 119.23 ± 16.48 Pa, fibrin/HA 202.3 ± 17.33 Pa; Fig. 3b). These findings indicate that the bulk mechanical properties of fibrin and combination scaffolds are within the optimal stiffness range (100–1000 Pa) for CNS tissue and for supporting NSPC proliferation and neuronal differentiation [76,77].

Confocal reflection microscopy was used to assess the micro-architecture of the fibrin and combination hydrogels since the hydrogel remains fully hydrated without fixation in this method, thus preserving native structure [61,62]. The fibrin network was visualized with a confocal microscope by scanning with a 488 nm laser and collecting the light reflected back from the hydrogel. We found fibrin fibers easier to visualize in fibrin hydrogels, while the fibrin in combination hydrogels appeared intermixed with less reflective material (Fig. S2). HA has high water content and thus may have a low reflective signal in confocal reflection microscopy since a large difference in refractive index between the material and water is required to obtain a strong signal with this method. Hydrated HA may surround fibrin fibers in the combination hydrogels, partially masking reflection and inhibiting clear visualization of individual fibers.

3.3. HNSPCs proliferate and differentiate within combination scaffolds

The proliferative capacity of hNSPCs within fibrin and combination scaffolds was assessed to gauge scaffold ability to support hNSPC function. HNSPCs proliferate similarly well in

fibrin and combination scaffolds with HA and HA/laminin, as evaluated by Ki-67 immunostaining to detect cycling cells not in G_0-phase of the cell cycle (Fig. 4). There was a slight but not significant trend of increased hNSPC proliferation within scaffolds that included HA and laminin over scaffolds of fibrin alone, indicating that at a minimum HA and laminin do not inhibit cell proliferation. EdU-incorporation to mark proliferating cells in S-phase revealed a matching trend in that more proliferating hNSPCs were present in combination scaffolds than fibrin scaffolds after 7 days of culture (EdU-positive cells in fibrin 10.74 ± 1.54%, fibrin/HA 13.55 ± 1.52%, fibrin/HA/lam 13.62 ± 4.04%). These values are similar to those of cells cultured on laminin-coated glass, indicating that scaffolds enable hNSPC proliferation [78].

An important characteristic of scaffolds is the ability to promote differentiation of transplanted stem cells since differentiated cells may stimulate repair of the host tissue. For this reason, we investigated differentiation of hNSPCs into neurons and astrocytes within the various scaffolds. We observed differentiation of hNSPCs into astrocytes within fibrin, fibrin/HA, and fibrin/HA/lam scaffolds, as assessed by immunostaining for the astrocyte marker glial fibrillary acidic protein (GFAP) (Fig. 5a). HNSPCs also formed neurons positive for the early neuronal marker doublecortin within all three scaffolds (Fig. 5b). Immunostaining is not uniform throughout the gels, making quantitative analysis of differentiated cells impractical. Interestingly, neurite outgrowth from differentiated neurons was most robust in combination scaffolds containing laminin (Fig. 5b right). Some differentiated neurons within the combination scaffolds were double-positive for doublecortin and the more mature neuronal marker, microtubule-associated protein 2 (MAP2) (Fig. S3). These data indicate that combination scaffolds can support hNSPC proliferation and differentiation, providing rationale for their use as transplant constructs to restore injured CNS tissue.

3.4. hNSPCs express fibrinogen- and laminin-binding integrins

The proliferation, differentiation, and elongation of hNSPCs within scaffolds containing fibrin and laminin ECM suggest these cells express ECM-binding integrin α and β subunits. RNA Sequencing (RNA-Seq) was utilized to determine the types of integrins expressed by hNSPCs and indicated high levels of mRNA for β1, α7, α3, α6, β5, αV, α5, and α9 integrins (Fig. 6a, b). These integrins primarily bind fibrinogen (Fig. 6c), laminin, fibronectin, tenascin, osteopontin, and vitronectin [79–81]. The only fibrinogen-binding integrins expressed by hNSPCs at high or moderate levels in the RNA-Seq data are αVβ1 and α5β1 (Fig. 6c). In agreement with the RNA data presented here, we previously found by flow cytometry that hNSPCs express the α5 integrin subunit (~56% positive), and also the laminin-binding integrins β1, α7, α 6, and α3 [34]. However, our previous analysis did not include αV, so flow cytometry was used to determine that ~54% of the hNSPC population expresses cell surface αV (Fig. 6d). Therefore, after using RNA-Seq to assess expression levels of all integrins and flow cytometry to determine cell surface expression, we conclude that hNSPCs likely interact with fibrinogen in scaffolds through αVβ1 and α5β1 integrins and with laminin via α7β1, α6β1, α6β4, and α3β1.

Interaction of HA with cells is mediated by several receptors, including CD44 [82], RHAMM [83], and ICAM1 [84]. However, HA is not always sufficient for cell adhesion [32,33], and in our study hNSPCs do not bind to HA alone but require addition of a cell adhesion molecule or peptide to mediate binding (Fig. S4). We assessed HA receptors by RNA-Seq and found the following levels of expression: CD44 (high, avg. RPKM 316.7), TLR4 (high, avg. RPKM 69.13), RHAMM (high, avg. RPKM 16.8), layilin (low-moderate, avg. RPKM 1.69), ICAM1 (low-moderate, avg. RPKM 1.57), TLR2 (none, avg. RPKM 0.02), lymphatic vessel endothelial hyaluronan receptor 1 (none, avg. RPKM 0.02). Thus, hNSPCs express several receptors known to bind HA though they are not sufficient to induce adhesion of these cells.

3.5. Hyaluronic acid slows hNSPC-mediated degradation of salmon fibrin in vitro

Degradation kinetics is another pivotal component of biomaterial design that can determine the efficacy of scaffolds for transplanted cells [68]. The inclusion of HA increased the polymerization efficiency and mechanical strength of the hydrogels as mentioned previously, so we tested whether it would affect hNSPC-mediated scaffold degradation. Since all the scaffolds contain a fibrin mesh, degradation was assessed by measuring the release of soluble fibrinogen from the cell-seeded scaffolds after a period of time in culture. HNSPCs were cultured in proliferating conditions within fibrin, fibrin/HA, fibrin/HA/lam scaffolds and degradation was measured using Western blot analysis of salmon fibrinogen released from the scaffold into the culture media over time (Fig. 7a).

The inclusion of HA in the scaffolds significantly reduced hNSPC-mediated scaffold degradation (Fig. 7). After 7 days in culture, there was approximately 7-fold more soluble fibrinogen present in the media of the fibrin compared to fibrin/HA scaffolds relative to hydrogels without cells seeded (Fig. 7b). As the concentration of cells seeded within the fibrin scaffolds increased, there was an increase in the amount of fibrinogen released into the culture media after 7 days. In contrast, higher cell concentrations did not stimulate a significant increase in the amount of soluble fibrinogen released from fibrin/HA scaffolds (Fig. 7c). The same amount of conditioned media was loaded for each sample and equal loading was confirmed by Ponceau S staining of all proteins in each sample and immunoblotting for transferrin, a major protein component of the media (Figs. 7c and S5). We examined whether cell-mediated degradation would be exacerbated at longer time points such as 30 days, which is sufficient time for initial hNSPC differentiation *in vivo* [85]. The release of soluble fibrinogen is increased nearly 20-fold from fibrin scaffolds after 30 days relative to hydrogels without cells seeded, while the combination scaffolds released less than 3-fold as much fibrinogen (Figs. 7d and S6a). There was a significant increase in degradation of the fibrin scaffolds from the 7 day to 30 day time points, but strikingly this was not the case for scaffolds including HA or HA and laminin (Fig. 7d). The inclusion of laminin did not alter the degradation kinetics of the combination scaffolds (Fig. 7d). Ponceau S confirmed approximately equal protein loading across all samples (Fig. S6b).

3.6. hNSPCs and combination scaffolds increase human endothelial cell-derived vasculogenesis

In order to create a scaffold construct that mimics the neurovascular niche, promotes vascularization, and encourages synergistic cross-talk between neural and endothelial cells, we used fibrin alone or in combination with HA and laminin to co-culture hNSPCs with hECFC-ECs. Scaffolds of fibrin, HA, and laminin with hNSPCs significantly bolstered vessel formation. HECFC-EC-derived vessels were easily visible in the scaffolds with and without hNSPCs after 5 days in culture (Fig. 8a). Quantitative analysis included vessel area percentage and total vessel length to indicate vessel growth, and the number of branch points as a reflection of vessel network complexity. Fibrin/HA/lam scaffolds with both hECFC-ECs and hNSPCs yielded the highest vessel area percentage, defined as the area of a given field occupied by vessels (Fig. 8b). These scaffolds contained a significantly higher vessel area than fibrin with hECFC-ECs, fibrin with co-cultured hNSPCs and hECFC-ECs, or combination scaffolds with hECFC-ECs only. However, inclusion of hNSPCs with hECFC-ECs in fibrin scaffolds showed a significantly greater vessel area percentage than hECFC-ECs alone in fibrin, demonstrating the marked effect of hNSPCs on vascular network formation within the scaffolds.

Examination of total vessel length, defined as the length of the vessels per imaged field, further confirmed the findings from vessel area percentage. Fibrin/HA/lam and the inclusion of co-cultured hNSPCs and hECFC-ECs significantly enhanced total vessel length in comparison to hECFC-ECs cultured alone within fibrin or combination scaffolds (Fig. 8c). There was a significant increase in the vessel length of co-cultured hECFC-ECs in fibrin scaffolds compared to hECFC-ECs cultured alone in fibrin, suggesting that hNSPCs substantially affect the length of hECFC-EC-derived vessels, regardless of biomaterial composition.

The number of vessel branch points within the scaffolds was measured as an indicator of vascular complexity. We found that the fibrin/HA/lam scaffolds with co-cultured hNSPCs and hECFC-ECs contained significantly more branch points than those with hECFC-ECs only and fibrin scaffolds with hECFC-ECs (Fig. 8d). Indeed, there was a nearly 2-fold increase in vessel branch points in co-cultures within combination scaffolds compared to the hECFC-ECs cultured alone in fibrin, highlighting the synergistic effect of both HA and laminin with hNSPCs on vascular network complexity.

Since hNSPCs are likely affecting vasculogenesis through secretion of pro-angiogenic factors, we analyzed our RNA-Seq data for known angiogenic factors. We found that hNSPCs express high mRNA levels of several angiogenic factors likely to contribute to increased vasculogenesis of hECFC-ECs (Fig. 8e). We grouped the angiogenic factors into functional classes (growth factors, cytokines/chemokines, adhesion molecules/ECM, and proteases/inhibitors) and designated cutoffs for high, moderate, and low expression. Interestingly, a larger majority of the adhesion molecule/ECM angiogenic factors and proteases and inhibitors that modify the ECM screened for in hNSPCs were highly expressed (71% and 55%, respectively), while only 32% of the growth factors and 13% of the cytokines/chemokines were highly expressed (Fig. 8f–i), emphasizing the influence the matrix has on promoting angiogenesis. The Hughes lab previously identified SPARC

(secreted protein acidic and rich in cysteine), IGFBP7 (insulin-like growth factor binding protein 7), collagen type 1 alpha 1, TGF-βI (transforming growth factor β-induced protein ig-h3, Big-h3), fibronectin 1, HGF (hepatocyte growth factor), and PCOLCE (procollagen C-endopeptidase enhancer 1) secreted by stromal cells as essential for endothelial cell sprouting or lumen formation [86,87], and these factors are also highly expressed by hNSPCs (Fig. 8). In sum, we studied the effect of scaffold composition and the presence of hNSPCs on the ability of hECFC-ECs to form complex vessel networks and found that both play an integral role in promoting formation of new vessels. RNA-Seq revealed that hNSPCs express several factors involved in angiogenesis, many of which are constituents of the ECM, that likely facilitate increased vasculogenesis by hECFC-ECs.

4. Discussion

The development of biomaterial scaffolds that provide maximal support for hNSPC survival and function will likely improve the ability of these cells to successfully treat the damaged CNS. We report here on the establishment of a novel combination scaffold incorporating salmon fibrin, HA, and laminin and the results of multiple tests showing that the scaffold material properties, effects on hNSPCs, degradation rate after seeding with hNSPCs, and potential for vascularization make it a viable material for these cells. Initial studies demonstrated the benefits of including salmon fibrin in the scaffolds since it stimulates greater hNSPC proliferation than mammalian fibrin. The incorporation of HA and laminin with salmon fibrin yields hydrogels that polymerize more effectively and are slightly stiffer than fibrin alone, but ideally match the mechanical characteristics of CNS tissue. Combination scaffolds support the proliferation and differentiation of hNSPCs, which express integrins that moderate binding to fibrin and laminin, indicating the advantages of these materials as substrates for hNSPCs. Combination scaffolds have a significantly slower hNSPC-mediated degradation profile than fibrin, thus overcoming a limitation of fibrin as a single component scaffold. Co-cultures of hNSPCs and hECFC-ECs revealed that vessel formation and branching complexity were enhanced in combination scaffolds containing both cell types, indicating the ability of these scaffolds to support vascularization. Combination scaffolds thus fulfill key criteria for hNSPC scaffolds, including non-toxic polymerization, biocompatibility with hNSPCs, ability to be injected as a liquid then polymerize *in situ*, match the stiffness of the surrounding CNS tissue, reasonable degradation rate, and support for vascularization.

Salmon fibrin is a more effective biomaterial than mammalian fibrin for neuronal process extension, sprouting of human umbilical vein endothelial cells (HUVECs), functional recovery in a dorsal hemisection spinal cord injury model, and as shown here proliferation of hNSPCs [20,21,23]. The differences between salmon and mammalian fibrin may be attributed to species-specific variations in the fibrinogen sequence. Fibrinogen is a large glycoprotein containing pairs of three subunit chains Aα, Bβ, and γ. Fibrinogen chains are heavily glycosylated, and differences in carbohydrate modifications between salmon and mammalian fibrinogens may underlie some of the discrepancies between species, including variations in charge and solubility [20,24]. The salmon genome has recently been sequenced and comparison of the predicted amino acid sequences of salmon and mammalian (human and bovine) fibrinogen reveals discrepancies in the location of RGD sequences within the

chains. The salmon fibrinogen Aα and γ chains each contain one RGD sequence while both human and bovine Aα chains encode two RGDs with none in the γ chains. The salmon fibrinogen sequence is much more similar in this regard to the zebrafish fibrinogen sequence. The location differences in RGD sequences between salmon and mammalian fibrinogen might affect binding to cell surface integrins and in turn could be involved in differential integrin activation, which could influence a variety of cellular processes and explain the species-specific effects of salmon fibrin compared to mammalian fibrin.

Critical material properties for CNS scaffolds include polymerization kinetics that allow the scaffold and cells to be injected as a liquid and polymerize completely in the tissue and mechanical properties that match the soft tissue of the brain and spinal cord. The polymerization characteristics of the fibrin and combination scaffolds are similar since both are controlled by thrombin and the rate of polymerization can be modulated by adjusting the thrombin concentration, making fibrin-based scaffolds useful for CNS applications [16,23]. The combination scaffolds described in this study have polymerization kinetics suitable for cell transplantation and we are currently using these scaffolds with hNSPCs in an *in vivo* rodent model of ischemic stroke. We injected salmon fibrin as a hydrogel for spinal cord injury [23] and are now injecting the combination scaffold through a 30 gauge blunt tip needle into naïve and infarcted rat striatum. By utilizing thrombin at a concentration of 0.1 U/mL, we can inject 3 μL of scaffold/hNSPC solution at 1 μL/min without experiencing premature polymerization within the transplantation syringe. Thus, the polymerization kinetics of both fibrin and combination scaffolds are suitable for transplantation.

There was significantly less non-polymerized fibrinogen released from the combination hydrogels than the fibrin hydrogels 30 min after the onset of polymerization, suggesting more complete polymerization of the combination hydrogels (Fig. 2c). This may relate to differences between the two types of hydrogels in cross-link density and subsequent polymer trapping. An estimation of the distance between cross-links within the hydrogels can be obtained by employing the equation $G_o = \gamma kT$, where G_o is the low frequency elastic modulus and γ represents the number of polymeric network strands per unit volume [88]. For fibrin hydrogels the distance between cross-links is estimated to be 32.5 nm, while for the combination hydrogels the distance is lower at 27.3 nm due to the IPN of HA. The reduced distance between cross links in the combination scaffolds suggest there may be increased trapping of fibrinogen that prevents its escape during polymerization. This finding is similar to previous work illustrating decreased length between fiber nodes of collagen-fibrin IPN combination scaffolds compared to those of pure collagen [89].

The reduced cross-link distance in the combination scaffolds may be tied to substrate mechanics, which can affect NSPC differentiation and thus is an important parameter to consider for NSPC transplantation scaffolds [90]. NSPC differentiation is strongly influenced by substrate stiffness in ranges physiologically relevant for CNS tissue [91], such that soft substrates support neuronal differentiation while stiffer substrates induce generation of glia [72,73,92]. A mechanical stretch stimulus decreases NSPC differentiation into oligodendrocytes when the substrate is laminin, but not fibronectin, highlighting the importance of integrin signaling to substrate sensing [93]. HNSPCs express a stretch-activated ion channel, Piezo1, that responds to a variety of mechanical stimuli and guides

lineage choice towards neurons or astrocytes based on substrate stiffness [94]. The stiffness of the fibrin and combination hydrogels used here (~100–300 Pa) falls within the optimal range for supporting neurite branching [95], NSPC differentiation [72,73,92], and matches the compliance of human brain tissue (~100–1000 Pa) [25,91,96]. The scaffolds that include HA are slightly stiffer than those without HA, which may be due to a combination of factors including the increased cross-link density, potential cross-linking of thiols on the HA with cysteine residues on fibrinogen via disulfide bonding, and an increase in polymer mass from the HA. The polymerization kinetics and mechanical properties of combination scaffolds of fibrin and HA are optimal for hNSPCs and CNS tissue applications.

The rate of scaffold degradation to allow for proper cellular integration has been highlighted as an important component of scaffold design [97]. Although there is no consensus on the ideal residence time for an implanted scaffold, it is crucial for the scaffold to remain intact long enough to promote transplanted cell survival and incorporation into the host. It should be noted that as the scaffold degrades over time *in vivo*, its mechanical properties will change, and the microenvironment of the transplanted cells will be dominated by the host tissue rather than the scaffold. *In vitro*, salmon fibrin scaffolds seeded with mouse spinal cord neurons persist intact much longer than bovine fibrin or human fibrin scaffolds seeded with cells as measured by gross observation of the scaffolds [20]. Similarly, HUVECs degrade human fibrin more swiftly than salmon fibrin *in vitro* [21]. Despite salmon fibrin's reduced degradation in these *in vitro* studies, it degraded on the order of 7 days in the more complex *in vivo* environment of the injured rodent spinal cord [23], which would be too short to support the differentiation of hNSPCs *in vivo*, requiring a minimum of one month. Integration of HA with salmon fibrin to create combination scaffolds significantly attenuated cell-mediated fibrin degradation while the inclusion of laminin did not further affect degradation (Fig. 7). These findings suggest the IPN created by HA slows fibrin degradation, which may occur by several different mechanisms. The thiols on the HA may cross-link with cysteines on fibrinogen via disulfide bridges, rendering the combination scaffold less susceptible to degradation. HA may also bind plasmin and thus limit its diffusion. Plasmin is formed from plasminogen via enzymes termed plasminogen activators. Plasminogen activator expression by hNSPCs may also be reduced within the combination scaffolds due to the presence of HA, as HA can inhibit expression of plasminogen activator in human synovial fibroblasts [98]. Based on our RNA-Seq data, hNSPCs express the plasminogen activators, urokinase and tissue plasminogen activator, but do not express plasminogen. Plasminogen is present in the fibrin hydrogels since it co-purifies with fibrinogen [20,99]. Combining fibrin and HA to create a composite scaffold ameliorates the rapid cell-mediated degradation occurring with fibrin alone.

Scaffolds for hNSPCs should support basic cell functions, such as proliferation and differentiation, which in many cases will be mediated by binding to integrins on the cell surface. Each of the individual scaffold components (fibrin, HA, and laminin) encourage rodent and human NSPC proliferation *in vitro* and *in vivo* [16,34,39,60]. Thus it is not surprising that hNSPCs proliferate when cultured in combination scaffolds of these biomaterials (Fig. 4), suggesting these scaffolds may aid cell survival and expansion post-transplantation. Although laminin stimulated expansion of hNSPCs in a two-dimensional system [34,39], the addition of laminin to the combination scaffolds did not further increase

hNSPC proliferation. However, laminin may have more of an effect on neurite outgrowth of neurons differentiated from hNSPCs (Fig. 5b), which would fit with laminin's long-recognized role in the promotion of neurite outgrowth [34,100,101]. Fibrin and HA promote differentiation in other systems as scaffolds with growth factors support the differentiation of mouse and human NSPCs into neurons and glia *in vivo* [19] and HA/polylysine multilayer films encourage rat NSPC differentiation into neurons and glia *in vitro* [102]. Interactions between cells and ECM scaffolds are mediated by cell surface integrins [79] and hNSPCs express integrins to bind fibrin (αVβ1 and α5β1) and laminin (α7β1, α6β1, and α3β1) as shown by RNA-Seq analysis and flow cytometry (Fig. 6) [34] [80,81]. Combination scaffolds of fibrin and HA support hNSPCs and these cells have cell surface fibrinogen and laminin-binding integrins necessary for adhesion to the scaffolds.

An important characteristic of scaffolds is the ability to support vascularization and our data indicate combination scaffolds of fibrin, HA, and laminin encourage the formation of vessels from hECFC-ECs. Adding human NSPCs to hECFC-ECs within salmon fibrin-HA-laminin scaffolds significantly increases the formation of vascular structures (Fig. 8). Since for most measures of vessel formation there were not significant differences between the fibrin or combination scaffolds with hECFC-ECs alone, we conclude that the hNSPCs have a more dominant effect on vessel generation than the biomaterial composition. The vessels we observed from hECFC-ECs are not fully developed vascular structures. Further vessel maturation and stabilization would require the addition of perivascular cells to facilitate anastomosis and increase survival of networks, which we plan to explore in future work. Overall, our data indicate a strong synergistic effect of human neural stem cells and biomaterials on the formation of human vessels.

Similar effects of NSPCs on formation of vessels from endothelial cells have been described for rodent cells, but not for human cells to our knowledge. Co-transplantation of mouse NSPCs and mouse ES-derived vascular progenitor cells without a scaffold into rodent stroke models leads to enhanced vessel formation in the infarct area [46]. Mouse NSPCs induce more vessel/cord formation from mouse brain periventricular endothelial cells when both cell types are co-cultured on Matrigel [41]. Co-transplants of mouse NSPCs and mouse endothelial cells in a synthetic poly(ethylene glycol)-based scaffold implanted subcutaneously generated better vessel formation than transplants of endothelial cells alone in the scaffolds [47]. Using the same scaffold and cells in a rat model of spinal cord injury, the greatest degree of vessel formation occurred in the scaffold containing both mouse NSPCs and endothelial cells [53]. Our data now add to this literature by demonstrating similar effects of human NSPCs on human endothelial cell vessel formation.

The effect of hNSPCs on vasculogenesis by hECFC-ECs may be due to neural cell secreted factors acting on the hECFC-ECs. RNA-seq analysis of the hNSPCs shows high expression of multiple genes relevant for vasculogenesis (Fig. 8). The vasculogenic factors assessed in the RNA-seq data comprise a broad class of growth factors, cytokines/chemokines, adhesion molecules and ECM, and proteases and inhibitors. A large percentage of the factors in the adhesion molecule/ECM and proteases/inhibitors categories were highly expressed (71% and 55%, respectively), suggesting that a significant component of the effect of hNSPCs on vasculogenesis may be mediated by modifying the ECM. In particular, hNSPCs produce

collagen I and IV, laminin, and fibronectin as well as the proteases MMP2, MMP15, plasminogen activator (PLAU), MMP14, and the protease inhibitors TIMP2 and TIMP1 (Fig. 8). In addition to factors that modify the ECM, hNSPCs express high levels of the growth factors VEGF, PDGF, and TGF-β1 (Fig. 8), all of which are factors essential for angiogenesis [103–105]. Rodent NSPCs express VEGF-A *in vitro*, and *in vivo* production of VEGF-A has been demonstrated for mouse hippocampal NSPCs [106–108]. Human NSPCs transplanted into a rodent stroke model promote behavioral recovery and neovascularization, and both of these effects are lost if VEGF is blocked with a human VEGF-specific antibody [109]. Here, we add to these findings by providing direct evidence of VEGF-A and VEGF-B mRNA production by hNSPCs. We showed previously that the growth factors TGF-α, HGF, and the ECM molecule fibronectin, all of which are expressed by hNSPCs, are secreted by fibroblasts and contribute to angiogenic sprouting from endothelial cells [86,87]. Intriguingly, hNSPCs also express elevated levels of SPARC, IGFBP7, collagen I, TGF-βI (βig-h3), and moderate levels of PCOLCE, each of which the Hughes lab found to be required for endothelial cell lumen formation, which relates to vessel formation and maturation [86]. These data suggest that factors produced by the hNSPCs are likely playing a key role in increasing vasculogenesis in co-cultures with hECFC-ECs, highlighting the relevance of crosstalk between neural and endothelial cells for vascularization.

Interest in the use of scaffolds containing multiple components is growing in the fields of tissue engineering and regenerative medicine. Scaffolds combining fibrin and hyaluronic acid induce greater chondrogenesis of human bone marrow-derived mesenchymal stem cells (BMSCs) *in vitro* than fibrin scaffolds [110]. Human MSCs and human umbilical vein endothelial cells (HUVECs) were plated in scaffolds of fibrin or collagen/fibrin combinations at different mass ratios to assess vascularization [111]. In this case, the ratio of components in the combination scaffold played a key role in its effect on cells. Vessel formation was best in either fibrin or combination scaffolds at a mass ratio of 40/60 (collagen/fibrin); notably the individual and combinations scaffolds were of similar stiffness with combination scaffolds having more robust polymerization kinetics than those of fibrin alone. MSCs coalesced along vessels in the 40/60 combination scaffolds, but specific effects of the scaffold on MSCs were not assessed. Combination scaffolds have been utilized to provide a localized source of therapeutic molecules, as fibrin-HA IPNs loaded with SDF-1α promote homing of chondrogenic progenitor cells and subsequent functional repair of bovine cartilage [112]. In regards to NSPCs, HA-collagen scaffolds increase mouse NSPC survival when transplanted into the infarct core of stroke-injured mice [9]. Our study now identifies combination scaffolds of fibrin-HA-laminin as beneficial scaffolds for human NSPCs since they resist rapid degradation, enhance vascularization by hECFC-ECs, and support hNSPC proliferation and differentiation. Based on the promising results to date with combination scaffolds, more research is clearly warranted to test the effects of a variety of combination scaffolds on human NSPCs as these cells move toward use in clinical applications.

5. Conclusions

Our data indicate that combination scaffolds consisting of salmon fibrin with HA and laminin possess material properties that enable polymerization with cells, mimic native brain

tissue, support hNSPC function, and better resist degradation than fibrin alone. Furthermore, hNSPCs work synergistically with combination scaffolds to enhance vasculogenesis from hECFC-ECs, thus providing motivation for their use to create vascularized transplant scaffold constructs to treat human disease. Our findings offer implications for the use of more complex neural tissue engineering strategies utilizing multiple human cell types and scaffold biomaterials to enhance cellular function *in vitro* and *in vivo*. Employment of more sophisticated methods such as combination scaffolds to increase stem cell survival and function post-transplant will be critical for their use as cellular therapeutics.

Supplementary Material

Refer to Web version on PubMed Central for supplementary material.

Acknowledgments

The authors would like to thank Dr. Evelyn Sawyer and Sea Run Holdings Inc. for the gift of salmon fibrinogen and thrombin; Dr. Phillip Schwartz for providing hNSPCs; the laboratories of Drs. Szu Wang and Nancy Da Silva for assistance in obtaining rheological measurements; Rylan Kautz and Andrew Yale for assistance in designing the graphical abstract; UCI Genomics Core for RNA Sequencing. This work was supported by the National Institute of Neurological Disorders and Stroke (T32 NS082174, predoctoral fellowship to JA), the California Institute for Regenerative Medicine (RB5-07254, LAF), the Craig H. Neilsen Foundation (SCIRTS-296387, LAF), the National Center for Research Resources and the National Center for Advancing Translational Sciences, National Institutes of Health, through Grant UL1 TR001414 (Pilot Grant to LAF), and the National Institute of Health (R01 PQD5-CA180122, CCWH). CCWH also receives support from the Chao Family Comprehensive Cancer Center through a National Cancer Institute Center Grant (P30A062203).

Appendix A. Supplementary data

Supplementary data associated with this article can be found, in the online version, at http://dx.doi.org/10.1016/j.actbio.2016.07.043.

References

1. Lindvall O, Kokaia Z. Stem cells for the treatment of neurological disorders. Nature. 2006; 441(7097):1094–1096. [PubMed: 16810245]
2. Gage FH. Mammalian neural stem cells. Science. 2000; 287(5457):1433–1438. [PubMed: 10688783]
3. Kelly S, Bliss TM, Shah AK, Sun GH, Ma M, Foo WC, Masel J, Yenari MA, Weissman IL, Uchida N, Palmer T, Steinberg GK. Transplanted human fetal neural stem cells survive, migrate, and differentiate in ischemic rat cerebral cortex. Proc Natl Acad Sci USA. 2004; 101(32):11839–11844. [PubMed: 15280535]
4. Hayashi J, Takagi Y, Fukuda H, Imazato T, Nishimura M, Fujimoto M, Takahashi J, Hashimoto N, Nozaki K. Primate embryonic stem cell-derived neuronal progenitors transplanted into ischemic brain. J Cereb Blood Flow Metab. 2006; 26(7):906–914. [PubMed: 16395293]
5. Ikeda R, Kurokawa M, Chiba S, Yoshikawa H, Ide M, Tadokoro M, Nito S, Nakatsuji N, Kondoh Y, Nagata K, Hashimoto T, Suzuki N. Transplantation of neural cells derived from retinoic acid-treated cynomolgus monkey embryonic stem cells successfully improved motor function of hemiplegic mice with experimental brain injury. Neurobiol Dis. 2005; 20(1):38–48. [PubMed: 16137565]
6. McCreedy DA, Wilems TS, Xu H, Butts JC, Brown CR, Smith AW, Sakiyama-Elbert SE. Survival, differentiation, and migration of high-purity mouse embryonic stem cell-derived progenitor motor neurons in fibrin scaffolds after sub-acute spinal cord injury. Biomater Sci. 2014; 2(11):1672–1682. [PubMed: 25346848]

7. Burns T, Verfaillie C, Low W. Stem cells for ischemic brain injury: a critical review. J Comp Neurol. 2009; 515(1):125–144. [PubMed: 19399885]
8. Bliss T, Guzman R, Daadi M, Steinberg G. Cell transplantation therapy for stroke. Stroke. 2007; 38:817–826. [PubMed: 17261746]
9. Zhong J, Chan A, Morad L, Kornblum H, Fan G, Carmichael S. Hydrogel matrix to support stem cell survival after brain transplantation in stroke. Neurorehabil Neural Repair. 2010; 24(7):636–644. [PubMed: 20424193]
10. Tate CC, Shear DA, Tate MC, Archer DR, Stein DG, LaPlaca MC. Laminin and fibronectin scaffolds enhance neural stem cell transplantation into the injured brain. J Tissue Eng Regen Med. 2009; 3(3):208–217. [PubMed: 19229887]
11. Evans N, Gentleman E, Polak J. Scaffolds for stem cells. Mater Today. 2006; 9(12):26–33.
12. Zhang J, Tokatlian T, Zhong J, Ng Q, Patterson M, Lowry W, Carmichael S, Segura T. Physically associated synthetic hydrogels with long-term covalent stabilization for cell culture and stem cell transplantation. Adv Mater. 2011; 23(43):5098–5103. [PubMed: 21997799]
13. Willerth, SM., Sakiyama-Elbert, SE. Combining stem cells and biomaterial scaffolds for constructing tissues and cell delivery. StemBook. 2008. http://dx.doi.org/10.3824/stembook.1.1.1
14. Skop NB, Calderon F, Cho CH, Gandhi CD, Levison SW. Improvements in biomaterial matrices for neural precursor cell transplantation. Mol Cell Ther. 2014; 2:19. [PubMed: 26056586]
15. Li X, Katsanevakis E, Liu X, Zhang N, Wen X. Engineering neural stem cell fates with hydrogel design for central nervous system regeneration. Prog Polym Sci. 2012; 37(8):1105–1129.
16. Johnson P, Tatara A, McCreedy D, Shiu A, Sakiyama-Elbert S. Tissue-engineered fibrin scaffolds containing neural progenitors enhance functional recovery in a subacute model of SCI. Soft Matter. 2010; 6(20):5127–5137. [PubMed: 21072248]
17. Johnson PJ, Tatara A, Shiu A, Sakiyama-Elbert SE. Controlled release of neurotrophin-3 and platelet-derived growth factor from fibrin scaffolds containing neural progenitor cells enhances survival and differentiation into neurons in a subacute model of SCI. Cell Transplant. 2010; 19(1): 89–101. [PubMed: 19818206]
18. Wilems TS, Pardieck J, Iyer N, Sakiyama-Elbert SE. Combination therapy of stem cell derived neural progenitors and drug delivery of anti-inhibitory molecules for spinal cord injury. Acta Biomater. 2015; 28:23–32. [PubMed: 26384702]
19. Lu P, Wang Y, Graham L, McHale K, Gao M, Wu D, Brock J, Blesch A, Rosenzweig ES, Havton LA, Zheng B, Conner JM, Marsala M, Tuszynski MH. Long-distance growth and connectivity of neural stem cells after severe spinal cord injury. Cell. 2012; 150(6):1264–1273. [PubMed: 22980985]
20. Ju YE, Janmey P, McCormick M, Sawyer E, Flanagan L. Enhanced neurite growth from mammalian neurons in three-dimensional salmon fibrin gels. Biomaterials. 2007; 28(12):2097–2108. [PubMed: 17258313]
21. Sieminski AL, Gooch KJ. Salmon fibrin supports an increased number of sprouts and decreased degradation while maintaining sprout length relative to human fibrin in an in vitro angiogenesis model. J Biomater Sci Polym Ed. 2004; 15(2):237–242. [PubMed: 15109101]
22. Prange MT, Margulies SS. Regional, directional, and age-dependent properties of the brain undergoing large deformation. J Biomech Eng. 2002; 124(2):244–252. [PubMed: 12002135]
23. Sharp K, Dickson A, Marchenko S, Yee K, Emery P, Laidmåe I, Uibo R, Sawyer E, Steward O, Flanagan L. Salmon fibrin treatment of spinal cord injury promotes functional recovery and density of serotonergic innervation. Exp Neurol. 2012; 235(1):345–356. [PubMed: 22414309]
24. Laidmäe I, McCormick ME, Herod JL, Pastore JJ, Salum T, Sawyer ES, Janmey PA, Uibo R. Stability, sterility, coagulation, and immunologic studies of salmon coagulation proteins with potential use for mammalian wound healing and cell engineering. Biomaterials. 2006; 27(34): 5771–5779. [PubMed: 16919721]
25. Uibo R, Laidmäe I, Sawyer E, Flanagan L, Georges P, Winer J, Janmey P. Soft materials to treat central nervous system injuries: evaluation of the suitability of non-mammalian fibrin gels. Biochim Biophys Acta. 2009; 1793(5):924–930. [PubMed: 19344675]
26. Preston M, Sherman LS. Neural stem cell niches: roles for the hyaluronan-based extracellular matrix. Front Biosci. 2011; 3:1165–1179.

27. Moshayedi P, Carmichael ST. Hyaluronan, neural stem cells and tissue reconstruction after acute ischemic stroke. Biomatter. 2013; 3(1):e23863. [PubMed: 23507922]
28. Khaing ZZ, Milman BD, Vanscoy JE, Seidlits SK, Grill RJ, Schmidt CE. High molecular weight hyaluronic acid limits astrocyte activation and scar formation after spinal cord injury. J Neural Eng. 2011; 8(4):046033. [PubMed: 21753237]
29. Margolis RU, Margolis RK, Chang LB, Preti C. Glycosaminoglycans of brain during development. Biochemistry. 1975; 14(1):85–88. [PubMed: 122810]
30. Khaing ZZ, Seidlits SK. Hyaluronic acid and neural stem cells: implications for biomaterial design. J Mater Chem B. 2015; 3(40):7850–7866.
31. Lam J, Lowry WE, Carmichael ST, Segura T. Delivery of iPS-NPCs to the stroke cavity within a hyaluronic acid matrix promotes the differentiation of transplanted cells. Adv Funct Mater. 2014; 24(44):7053–7062. [PubMed: 26213530]
32. Chopra A, Lin V, McCollough A, Atzet S, Prestwich GD, Wechsler AS, Murray ME, Oake SA, Kresh JY, Janmey PA. Reprogramming cardiomyocyte mechanosensing by crosstalk between integrins and hyaluronic acid receptors. J Biomech. 2012; 45(5):824–831. [PubMed: 22196970]
33. Chopra A, Murray ME, Byfield FJ, Mendez MG, Halleluyan R, Restle DJ, Raz-Ben Aroush D, Galie PA, Pogoda K, Bucki R, Marcinkiewicz C, Prestwich GD, Zarembinski TI, Chen CS, Puré E, Kresh JY, Janmey PA. Augmentation of integrin-mediated mechanotransduction by hyaluronic acid. Biomaterials. 2014; 35(1):71–82. [PubMed: 24120037]
34. Flanagan L, Rebaza L, Derzic S, Schwartz P, Monuki E. Regulation of human neural precursor cells by laminin and integrins. J Neurosci Res. 2006; 83(5):845–856. [PubMed: 16477652]
35. Stabenfeldt SE, García AJ, LaPlaca MC. Thermoreversible laminin-functionalized hydrogel for neural tissue engineering. J Biomed Mater Res A. 2006; 77(4):718–725. [PubMed: 16555267]
36. Junka R, Valmikinathan CM, Kalyon DM, Yu X. Laminin functionalized biomimetic nanofibers for nerve tissue engineering. J Biomater Tissue Eng. 2013; 3(4):494–502. [PubMed: 24083073]
37. Jin K, Mao X, Xie L, Galvan V, Lai B, Wang Y, Gorostiza O, Wang X, Greenberg DA. Transplantation of human neural precursor cells in Matrigel scaffolding improves outcome from focal cerebral ischemia after delayed postischemic treatment in rats. J Cereb Blood Flow Metab. 2010; 30(3):534–544. [PubMed: 19826433]
38. Addington CP, Heffernan JM, Millar-Haskell CS, Tucker EW, Sirianni RW, Stabenfeldt SE. Enhancing neural stem cell response to SDF-1α gradients through hyaluronic acid-laminin hydrogels. Biomaterials. 2015; 72:11–19. [PubMed: 26340314]
39. Hall PE, Lathia JD, Caldwell MA, Ffrench-Constant C. Laminin enhances the growth of human neural stem cells in defined culture media. BMC Neurosci. 2008; 9:71. [PubMed: 18651950]
40. Calvo CF, Fontaine RH, Soueid J, Tammela T, Makinen T, Alfaro-Cervello C, Bonnaud F, Miguez A, Benhaim L, Xu Y, Barallobre MJ, Moutkine I, Lyytikkä J, Tatlisumak T, Pytowski B, Zalc B, Richardson W, Kessaris N, Garcia-Verdugo JM, Alitalo K, Eichmann A, Thomas JL. Vascular endothelial growth factor receptor 3 directly regulates murine neurogenesis. Genes Dev. 2011; 25(8):831–844. [PubMed: 21498572]
41. Vissapragada R, Contreras MA, da Silva CG, Kumar VA, Ochoa A, Vasudevan A, Selim MH, Ferran C, Thomas AJ. Bidirectional crosstalk between periventricular endothelial cells and neural progenitor cells promotes the formation of a neurovascular unit. Brain Res. 2014; 1565:8–17. [PubMed: 24675025]
42. Shen Q, Goderie SK, Jin L, Karanth N, Sun Y, Abramova N, Vincent P, Pumiglia K, Temple S. Endothelial cells stimulate self-renewal and expand neurogenesis of neural stem cells. Science. 2004; 304(5675):1338–1340. [PubMed: 15060285]
43. Sun J, Zhou W, Ma D, Yang Y. Endothelial cells promote neural stem cell proliferation and differentiation associated with VEGF activated Notch and Pten signaling. Dev Dyn. 2010; 239(9): 2345–2353. [PubMed: 20730910]
44. Tavazoie M, Van der Veken L, Silva-Vargas V, Louissaint M, Colonna L, Zaidi B, Garcia-Verdugo JM, Doetsch F. A specialized vascular niche for adult neural stem cells. Cell Stem Cell. 2008; 3(3):279–288. [PubMed: 18786415]
45. Nakagomi N, Nakagomi T, Kubo S, Nakano-Doi A, Saino O, Takata M, Yoshikawa H, Stern DM, Matsuyama T, Taguchi A. Endothelial cells support survival, proliferation, and neuronal

differentiation of transplanted adult ischemia-induced neural stem/progenitor cells after cerebral infarction. Stem Cells. 2009; 27(9):2185–2195. [PubMed: 19557831]

46. Li J, Tang Y, Wang Y, Tang R, Jiang W, Yang GY, Gao WQ. Neurovascular recovery via co-transplanted neural and vascular progenitors leads to improved functional restoration after ischemic stroke in rats. Stem Cell Rep. 2014; 3(1):101–114.
47. Ford MC, Bertram JP, Hynes SR, Michaud M, Li Q, Young M, Segal SS, Madri JA, Lavik EB. A macroporous hydrogel for the coculture of neural progenitor and endothelial cells to form functional vascular networks in vivo. Proc Natl Acad Sci USA. 2006; 103(8):2512–2517. [PubMed: 16473951]
48. Chen X, Aledia AS, Popson SA, Him L, Hughes CC, George SC. Rapid anastomosis of endothelial progenitor cell-derived vessels with host vasculature is promoted by a high density of cotransplanted fibroblasts. Tissue Eng Part A. 2010; 16(2):585–594. [PubMed: 19737050]
49. Chen X, Aledia AS, Ghajar CM, Griffith CK, Putnam AJ, Hughes CC, George SC. Prevascularization of a fibrin-based tissue construct accelerates the formation of functional anastomosis with host vasculature. Tissue Eng Part A. 2009; 15(6):1363–1371. [PubMed: 18976155]
50. White SM, Hingorani R, Arora RP, Hughes CC, George SC, Choi B. Longitudinal in vivo imaging to assess blood flow and oxygenation in implantable engineered tissues. Tissue Eng Part C Methods. 2012; 18(9):697–709. [PubMed: 22435776]
51. Shen Q, Wang Y, Kokovay E, Lin G, Chuang SM, Goderie SK, Roysam B, Temple S. Adult SVZ stem cells lie in a vascular niche: a quantitative analysis of niche cell-cell interactions. Cell Stem Cell. 2008; 3(3):289–300. [PubMed: 18786416]
52. Li Q, Ford MC, Lavik EB, Madri JA. Modeling the neurovascular niche: VEGF- and BDNF-mediated cross-talk between neural stem cells and endothelial cells: an in vitro study. J Neurosci Res. 2006; 84(8):1656–1668. [PubMed: 17061253]
53. Rauch MF, Hynes SR, Bertram J, Redmond A, Robinson R, Williams C, Xu H, Madri JA, Lavik EB. Engineering angiogenesis following spinal cord injury: a coculture of neural progenitor and endothelial cells in a degradable polymer implant leads to an increase in vessel density and formation of the blood-spinal cord barrier. Eur J Neurosci. 2009; 29(1):132–145. [PubMed: 19120441]
54. Schwartz PH, Bryant PJ, Fuja TJ, Su H, O'Dowd DK, Klassen H. Isolation and characterization of neural progenitor cells from post-mortem human cortex. J Neurosci Res. 2003; 74(6):838–851. [PubMed: 14648588]
55. Yuan SH, Martin J, Elia J, Flippin J, Paramban RI, Hefferan MP, Vidal JG, Mu Y, Killian RL, Israel MA, Emre N, Marsala S, Marsala M, Gage FH, Goldstein LS, Carson CT. Cell-surface marker signatures for the isolation of neural stem cells, glia and neurons derived from human pluripotent stem cells. PLoS ONE. 2011; 6(3):e17540. [PubMed: 21407814]
56. Melero-Martin JM, Khan ZA, Picard A, Wu X, Paruchuri S, Bischoff J. In vivo vasculogenic potential of human blood-derived endothelial progenitor cells. Blood. 2007; 109(11):4761–4768. [PubMed: 17327403]
57. Shu XZ, Liu Y, Luo Y, Roberts MC, Prestwich GD. Disulfide cross-linked hyaluronan hydrogels. Biomacromolecules. 2002; 3(6):1304–1311. [PubMed: 12425669]
58. Zheng Shu X, Liu Y, Palumbo FS, Luo Y, Prestwich GD. In situ crosslinkable hyaluronan hydrogels for tissue engineering. Biomaterials. 2004; 25(7–8):1339–1348. [PubMed: 14643608]
59. Struve J, Maher PC, Li YQ, Kinney S, Fehlings MG, Kuntz C, Sherman LS. Disruption of the hyaluronan-based extracellular matrix in spinal cord promotes astrocyte proliferation. Glia. 2005; 52(1):16–24. [PubMed: 15892130]
60. Liang Y, Walczak P, Bulte J. The survival of engrafted neural stem cells within hyaluronic acid hydrogels. Biomaterials. 2013; 34(22):5521–5529. [PubMed: 23623429]
61. Kotlarchyk MA, Botvinick EL, Putnam AJ. Characterization of hydrogel microstructure using laser tweezers particle tracking and confocal reflection imaging. J Phys: Condens Matter. 2010; 22(19): 194121. [PubMed: 20877437]
62. Hartmann A, Boukamp P, Friedl P. Confocal reflection imaging of 3D fibrin polymers. Blood Cells Mol Dis. 2006; 36(2):191–193. [PubMed: 16488165]

63. Zudaire E, Gambardella L, Kurcz C, Vermeren S. A computational tool for quantitative analysis of vascular networks. PLoS ONE. 2011; 6(11):e27385. [PubMed: 22110636]
64. Lissner MM, Thomas BJ, Wee K, Tong AJ, Kollmann TR, Smale ST. Age-related gene expression differences in monocytes from human neonates, young adults, and older adults. PLoS ONE. 2015; 10(7):e0132061. [PubMed: 26147648]
65. Goecks J, Nekrutenko A, Taylor J, G. Team. Galaxy: a comprehensive approach for supporting accessible, reproducible, and transparent computational research in the life sciences. Genome Biol. 2010; 11(8):R86. [PubMed: 20738864]
66. Trapnell C, Williams BA, Pertea G, Mortazavi A, Kwan G, van Baren MJ, Salzberg SL, Wold BJ, Pachter L. Transcript assembly and quantification by RNA-Seq reveals unannotated transcripts and isoform switching during cell differentiation. Nat Biotechnol. 2010; 28(5):511–515. [PubMed: 20436464]
67. Mortazavi A, Williams BA, McCue K, Schaeffer L, Wold B. Mapping and quantifying mammalian transcriptomes by RNA-Seq. Nat Methods. 2008; 5(7):621–628. [PubMed: 18516045]
68. Straley KS, Foo CW, Heilshorn SC. Biomaterial design strategies for the treatment of spinal cord injuries. J Neurotrauma. 2010; 27(1):1–19. [PubMed: 19698073]
69. Anlar B, Atilla P, Cakar AN, Kose MF, Beksaç MS, Dagdeviren A, Akçören Z. Expression of adhesion and extracellular matrix molecules in the developing human brain. J Child Neurol. 2002; 17(9):707–713. [PubMed: 12503652]
70. Georges-Labouesse E, Mark M, Messaddeq N, Gansmüller A. Essential role of alpha 6 integrins in cortical and retinal lamination. Curr Biol. 1998; 8(17):983–986. [PubMed: 9742403]
71. Kazanis I, Ffrench-Constant C. Extracellular matrix and the neural stem cell niche. Dev Neurobiol. 2011; 71(11):1006–1017. [PubMed: 21898854]
72. Saha K, Keung A, Irwin E, Li Y, Little L, Schaffer D, Healy K. Substrate modulus directs neural stem cell behavior. Biophys J. 2008; 95(9):4426–4438. [PubMed: 18658232]
73. Leipzig N, Shoichet M. The effect of substrate stiffness on adult neural stem cell behavior. Biomaterials. 2009; 30(36):6867–6878. [PubMed: 19775749]
74. Winter HH, Chambon F. Analysis of linear viscoelasticity of a crosslinking polymer at the gel point. J Rheol (1978-present). 1986; 30(2):367–382.
75. Calvet D, Wong JY, Giasson S. Rheological monitoring of polyacrylamide gelation: importance of cross-link density and temperature. Macromolecules. 2004; 37(20):7762–7771.
76. Banerjee A, Arha M, Choudhary S, Ashton R, Bhatia S, Schaffer D, Kane R. The influence of hydrogel modulus on the proliferation and differentiation of encapsulated neural stem cells. Biomaterials. 2009; 30(27):4695–4699. [PubMed: 19539367]
77. Aurand ER, Wagner J, Lanning C, Bjugstad KB. Building biocompatible hydrogels for tissue engineering of the brain and spinal cord. J Funct Biomater. 2012; 3(4):839–863. [PubMed: 24955749]
78. Lu J, Barrios C, Dickson A, Nourse J, Lee A, Flanagan L. Advancing practical usage of microtechnology: a study of the functional consequences of dielectrophoresis on neural stem cells. Integr Biol. 2012; 4(10):1223–1236.
79. Milner R, Campbell I. The integrin family of cell adhesion molecules has multiple functions within the CNS. J Neurosci Res. 2002; 69(3):286–291. [PubMed: 12125070]
80. Marshall JF, Rutherford DC, McCartney AC, Mitjans F, Goodman SL, Hart IR. Alpha v beta 1 is a receptor for vitronectin and fibrinogen, and acts with alpha 5 beta 1 to mediate spreading on fibronectin. J Cell Sci. 1995; 108(Pt 3):1227–1238. [PubMed: 7542669]
81. Suehiro K, Mizuguchi J, Nishiyama K, Iwanaga S, Farrell DH, Ohtaki S. Fibrinogen binds to integrin alpha(5)beta(1) via the carboxyl-terminal RGD site of the Aalpha-chain. J Biochem. 2000; 128(4):705–710. [PubMed: 11011154]
82. Lesley J, Hyman R, Kincade PW. CD44 and its interaction with extracellular matrix. Adv Immunol. 1993; 54:271–335. [PubMed: 8379464]
83. Turley EA, Austen L, Vandeligt K, Clary C. Hyaluronan and a cell-associated hyaluronan binding protein regulate the locomotion of ras-transformed cells. J Cell Biol. 1991; 112(5):1041–1047. [PubMed: 1705559]

84. McCourt PA, Ek B, Forsberg N, Gustafson S. Intercellular adhesion molecule-1 is a cell surface receptor for hyaluronan. J Biol Chem. 1994; 269(48):30081–30084. [PubMed: 7527024]
85. Tennstaedt A, Aswendt M, Adamczak J, Collienne U, Selt M, Schneider G, Henn N, Schaefer C, Lagouge M, Wiedermann D, Kloppenburg P, Hoehn M. Human neural stem cell intracerebral grafts show spontaneous early neuronal differentiation after several weeks. Biomaterials. 2015; 44:143–154. [PubMed: 25617134]
86. Newman AC, Nakatsu MN, Chou W, Gershon PD, Hughes CC. The requirement for fibroblasts in angiogenesis: fibroblast-derived matrix proteins are essential for endothelial cell lumen formation. Mol Biol Cell. 2011; 22(20):3791–3800. [PubMed: 21865599]
87. Newman AC, Chou W, Welch-Reardon KM, Fong AH, Popson SA, Phan DT, Sandoval DR, Nguyen DP, Gershon PD, Hughes CC. Analysis of stromal cell secretomes reveals a critical role for stromal cell-derived hepatocyte growth factor and fibronectin in angiogenesis, Arterioscler. Thromb Vasc Biol. 2013; 33(3):513–522.
88. Larson RG. The Structure and Rheology of Complex Fluids, Oxford University Press, New York. 1999
89. Rowe SL, Stegemann JP. Microstructure and mechanics of collagen-fibrin matrices polymerized using ancrod snake venom enzyme. J Biomech Eng. 2009; 131(6):061012. [PubMed: 19449966]
90. D'Angelo F, Tiribuzi R, Armentano I, Kenny JM, Martino S, Orlacchio A. Mechanotransduction: tuning stem cells fate. J Funct Biomater. 2011; 2(2):67–87. [PubMed: 24956164]
91. Tyler WJ. The mechanobiology of brain function. Nat Rev Neurosci. 2012; 13(12):867–878. [PubMed: 23165263]
92. Keung A, de Juan-Pardo E, Schaffer D, Kumar S. Rho GTPases mediate the mechanosensitive lineage commitment of neural stem cells. Stem Cells. 2011; 29(11):1886–1897. [PubMed: 21956892]
93. Arulmoli J, Pathak MM, McDonnell LP, Nourse JL, Tombola F, Earthman JC, Flanagan LA. Static stretch affects neural stem cell differentiation in an extracellular matrix-dependent manner. Sci Rep. 2015; 5:8499. [PubMed: 25686615]
94. Pathak MM, Nourse JL, Tran T, Hwe J, Arulmoli J, Le DT, Bernardis E, Flanagan LA, Tombola F. Stretch-activated ion channel Piezo1 directs lineage choice in human neural stem cells. Proc Natl Acad Sci USA. 2014; 111(45):16148–16153. [PubMed: 25349416]
95. Georges P, McCormick M, Flanagan L, Ju YE, Sawyer E, Janmey P. Tuning the elasticity of biopolymer gels for optimal wound healing. Mater Res Soc Symp Proc. 2005; 897E
96. Levental I, Georges PC, Janmey PA. Soft biological materials and their impact on cell function, Soft Matter 3 (3) (. 2007:299–306.
97. Dhandayuthapani B, Yoshida Y, Maekawa T, Kumar DS. Polymeric scaffolds in tissue engineering application: a review. Int J Polymer Sci. 2011; 2011:290602.
98. Nonaka T, Kikuchi H, Sohen S, Fukuda K, Hamanishi C, Tanaka S. Comparison of the inhibitory effects of two types (90 kDa and 190 kDa) of hyaluronic acid on the expression of fibrinolytic factors in human synovial fibroblasts. Mod Rheumatol. 2002; 12(2):160–166. [PubMed: 24383905]
99. Wang LZ, Gorlin J, Michaud SE, Janmey PA, Goddeau RP, Kuuse R, Uibo R, Adams D, Sawyer ES. Purification of salmon clotting factors and their use as tissue sealants. Thromb Res. 2000; 100(6):537–548. [PubMed: 11152934]
100. Lander AD, Fujii DK, Reichardt LF. Laminin is associated with the "neurite outgrowth-promoting factors" found in conditioned media. Proc Natl Acad Sci USA. 1985; 82(7):2183–2187. [PubMed: 3856891]
101. Hantaz-Ambroise D, Vigny M, Koenig J. Heparan sulfate proteoglycan and laminin mediate two different types of neurite outgrowth. J Neurosci. 1987; 7(8):2293–2304. [PubMed: 2956378]
102. Lee IC, Wu YC, Cheng EM, Yang WT. Biomimetic niche for neural stem cell differentiation using poly-L-lysine/hyaluronic acid multilayer films. J Biomater Appl. 2015; 29(10):1418–1427. [PubMed: 25502767]
103. Ferrara N. Role of vascular endothelial growth factor in regulation of physiological angiogenesis. Am J Physiol Cell Physiol. 2001; 280(6):C1358–C1366. [PubMed: 11350730]

104. Battegay EJ, Rupp J, Iruela-Arispe L, Sage EH, Pech M. PDGF-BB modulates endothelial proliferation and angiogenesis in vitro via PDGF beta-receptors. J Cell Biol. 1994; 125(4):917–928. [PubMed: 7514607]

105. Ferrari G, Cook BD, Terushkin V, Pintucci G, Mignatti P. Transforming growth factor-beta 1 (TGF-beta1) induces angiogenesis through vascular endothelial growth factor (VEGF)-mediated apoptosis. J Cell Physiol. 2009; 219(2):449–458. [PubMed: 19180561]

106. Kirby ED, Kuwahara AA, Messer RL, Wyss-Coray T. Adult hippocampal neural stem and progenitor cells regulate the neurogenic niche by secreting VEGF. Proc Natl Acad Sci USA. 2015; 112(13):4128–4133. [PubMed: 25775598]

107. Maurer MH, Tripps WK, Feldmann RE, Kuschinsky W. Expression of vascular endothelial growth factor and its receptors in rat neural stem cells. Neurosci Lett. 2003; 344(3):165–168. [PubMed: 12812831]

108. Mosher KI, Andres RH, Fukuhara T, Bieri G, Hasegawa-Moriyama M, He Y, Guzman R, Wyss-Coray T. Neural progenitor cells regulate microglia functions and activity. Nat Neurosci. 2012; 15(11):1485–1487. [PubMed: 23086334]

109. Horie N, Pereira MP, Niizuma K, Sun G, Keren-Gill H, Encarnacion A, Shamloo M, Hamilton SA, Jiang K, Huhn S, Palmer TD, Bliss TM, Steinberg GK. Transplanted stem cell-secreted vascular endothelial growth factor effects poststroke recovery, inflammation, and vascular repair. Stem Cells. 2011; 29(2):274–285. [PubMed: 21732485]

110. Snyder TN, Madhavan K, Intrator M, Dregalla RC, Park D. A fibrin/hyaluronic acid hydrogel for the delivery of mesenchymal stem cells and potential for articular cartilage repair. J Biol Eng. 2014; 8:10. [PubMed: 25061479]

111. Rao RR, Peterson AW, Ceccarelli J, Putnam AJ, Stegemann JP. Matrix composition regulates three-dimensional network formation by endothelial cells and mesenchymal stem cells in collagen/fibrin materials. Angiogenesis. 2012; 15(2):253–264. [PubMed: 22382584]

112. Yu Y, Brouillette MJ, Seol D, Zheng H, Buckwalter JA, Martin JA. Use of recombinant human stromal cell-derived factor 1α-loaded fibrin/hyaluronic acid hydrogel networks to achieve functional repair of full-thickness bovine articular cartilage via homing of chondrogenic progenitor cells. Arthritis Rheumatol. 2015; 67(5):1274–1285. [PubMed: 25623441]

Statement of Significance

Interest has increased recently in the development of biomaterials as neural stem cell transplantation scaffolds to treat central nervous system (CNS) injury since scaffolds improve survival and integration of transplanted cells. We report here on a novel combination scaffold composed of fibrin, hyaluronic acid, and laminin to support human neural stem/progenitor cell (hNSPC) function. This combined biomaterial scaffold has appropriate physical properties for hNSPCs and the CNS, supports hNSPC proliferation and differentiation, and attenuates rapid cell-mediated scaffold degradation. The hNSPCs and scaffold components synergistically encourage new vessel formation from human endothelial cells. This work marks the first report of a combination scaffold supporting human neural and vascular cells to encourage vasculogenesis, and sets a benchmark for biomaterials to treat CNS injury.

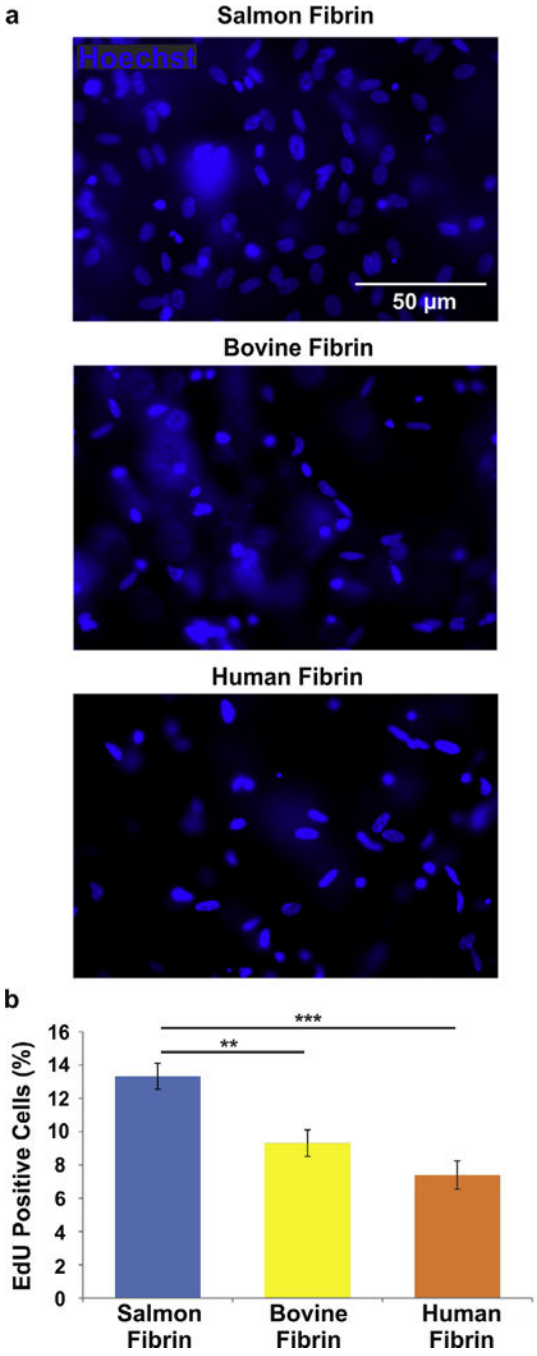

Fig. 1.

Salmon fibrin encourages greater hNSPC proliferation than bovine or human fibrin. HNSPCs (5×10^4) were seeded into scaffolds of salmon, bovine, or human fibrin and cells were analyzed after 6 days. (a) More hNSPCs are present in salmon fibrin than mammalian fibrin scaffolds (nuclei detected by Hoechst staining). (b) EdU-incorporation reveals a higher percentage of cells in S-phase of the cell cycle in salmon fibrin scaffolds than mammalian fibrin. P = 0.0023 (salmon vs. bovine), P = 2.5E−05 (salmon vs. human). $^{**}P < 0.01$, $^{***}P < 0.001$. Error bars represent SEM. N = 3 independent biological repeats.

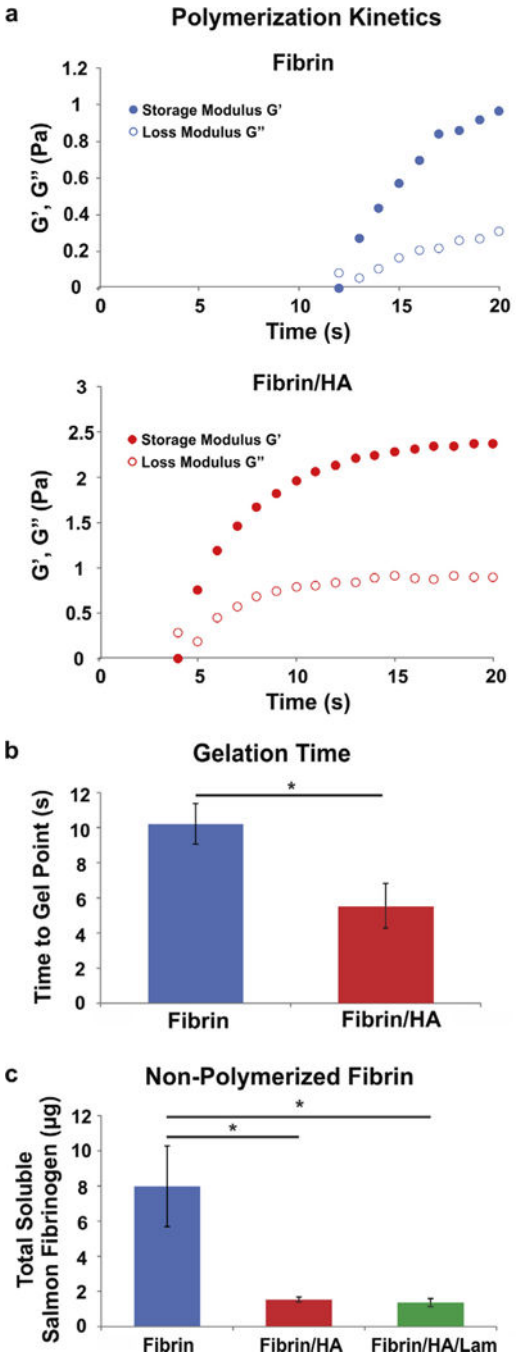

Fig. 2.

Increased gelation efficiency of combination hydrogels. (a) Polymerization of fibrin hydrogels (blue) and combination fibrin/HA hydrogels (red) was measured by oscillatory rheology. Storage modulus G′ (closed circles) and loss modulus G″ (open circles) over time illustrate the transition of the scaffold from a liquid to gel state. The transition occurs much more rapidly for fibrin/HA combination hydrogels. (b) The time to gel point, defined as the time at which G′ = G″ for each hydrogel, is approximately twice as long for fibrin (blue bar) as fibrin/HA hydrogels (red bar). P = 0.048. (c) The amount of soluble, non-

polymerized fibrinogen released into the media approximately 30 min after the onset of polymerization of hydrogels not seeded with cells is significantly higher for fibrin (blue bar) than combination hydrogels (red and green bars), revealing more complete polymerization of combination hydrogels. P = 0.048 (fibrin vs. fibrin/HA), P = 0.044 (fibrin vs. fibrin/HA/lam). $^{*}P < 0.05$. Error bars represent SEM. N = 3 independent biological repeats.

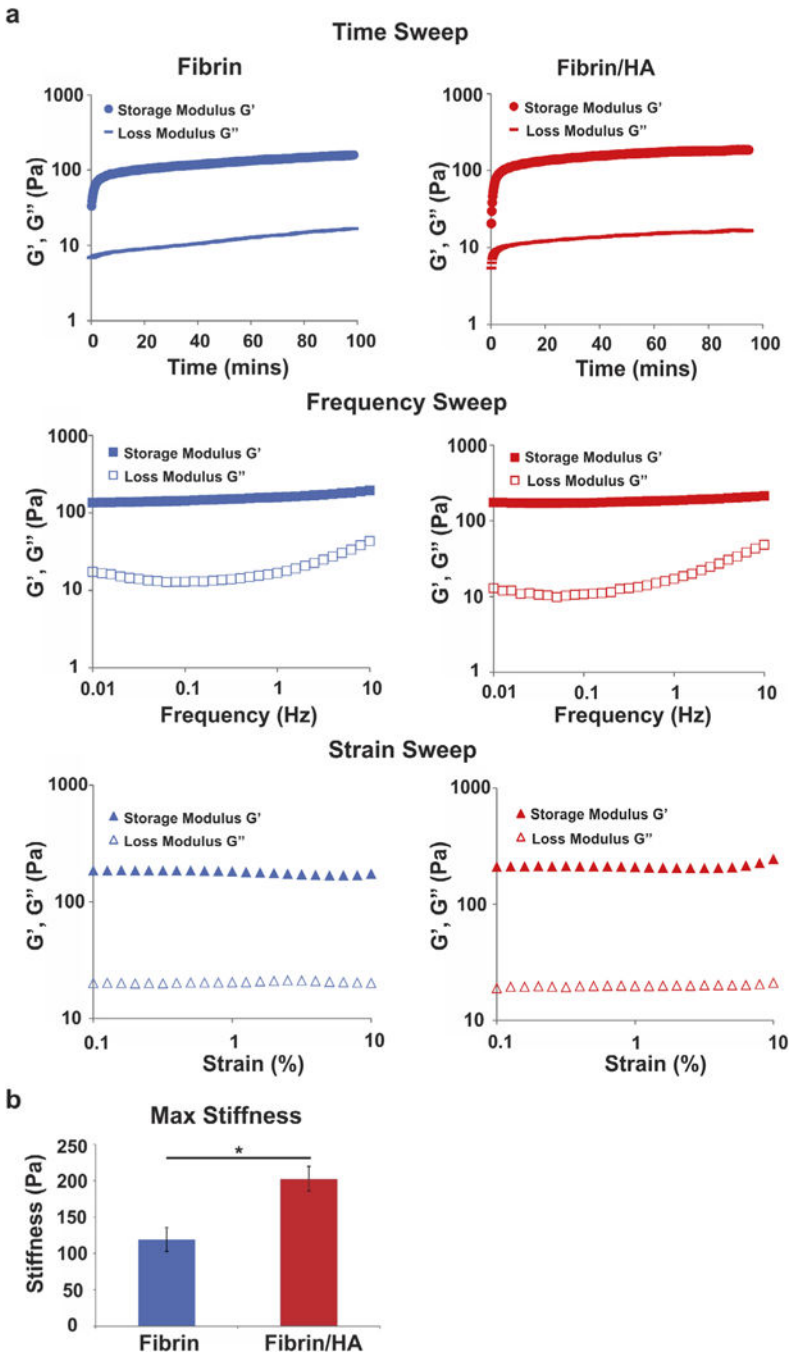

Fig. 3.

Combination scaffolds are stiffer than fibrin scaffolds but both are in the stiffness range of CNS tissue. (a) Oscillatory rheology was used to gather bulk mechanical properties of fibrin and fibrin/HA hydrogels. Storage modulus G′ (closed circles) and loss modulus G″ (closed dashes) over time illustrate the transition of the scaffold from a liquid to gel-like state for fibrin (blue) and fibrin/HA (red) hydrogels. Storage modulus G′ (closed squares and triangles) remains greater than the loss modulus G″ (open squares and triangles) over a broad range of frequencies and strains for both hydrogels (middle and bottom plots). (b) The

maximum hydrogel stiffness measured by the storage modulus G′ at 90 min indicates scaffolds with fibrin and HA (red bar) are significantly stiffer than those with fibrin alone (blue bar) although both are within 100–250 Pa. P = 0.026. *P < 0.05. Error bars represent SEM. N = 3 independent biological repeats.

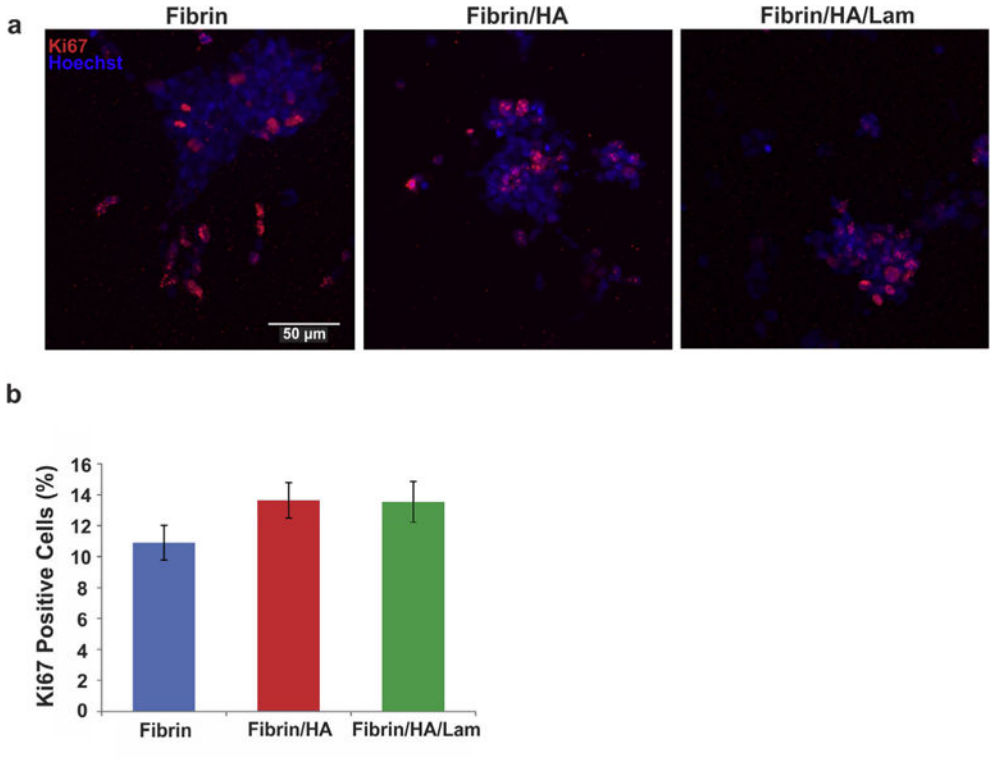

Fig. 4.

HNSPCs proliferate within combination scaffolds. (a) HNSPCs (1×10^5) were seeded into fibrin or combination scaffolds and proliferating cells not in G_0-phase of the cell cycle were detected by immunostaining for Ki67. (b) Ki67-positive nuclei were quantified after 3 days in proliferating conditions and indicate that inclusion of HA (red bar) and HA with laminin (green bar) is not detrimental to the hNSPCs as shown by similar proliferation of the cells in combination and fibrin scaffolds (blue bars). Error bars represent SEM. N = 3 independent biological repeats.

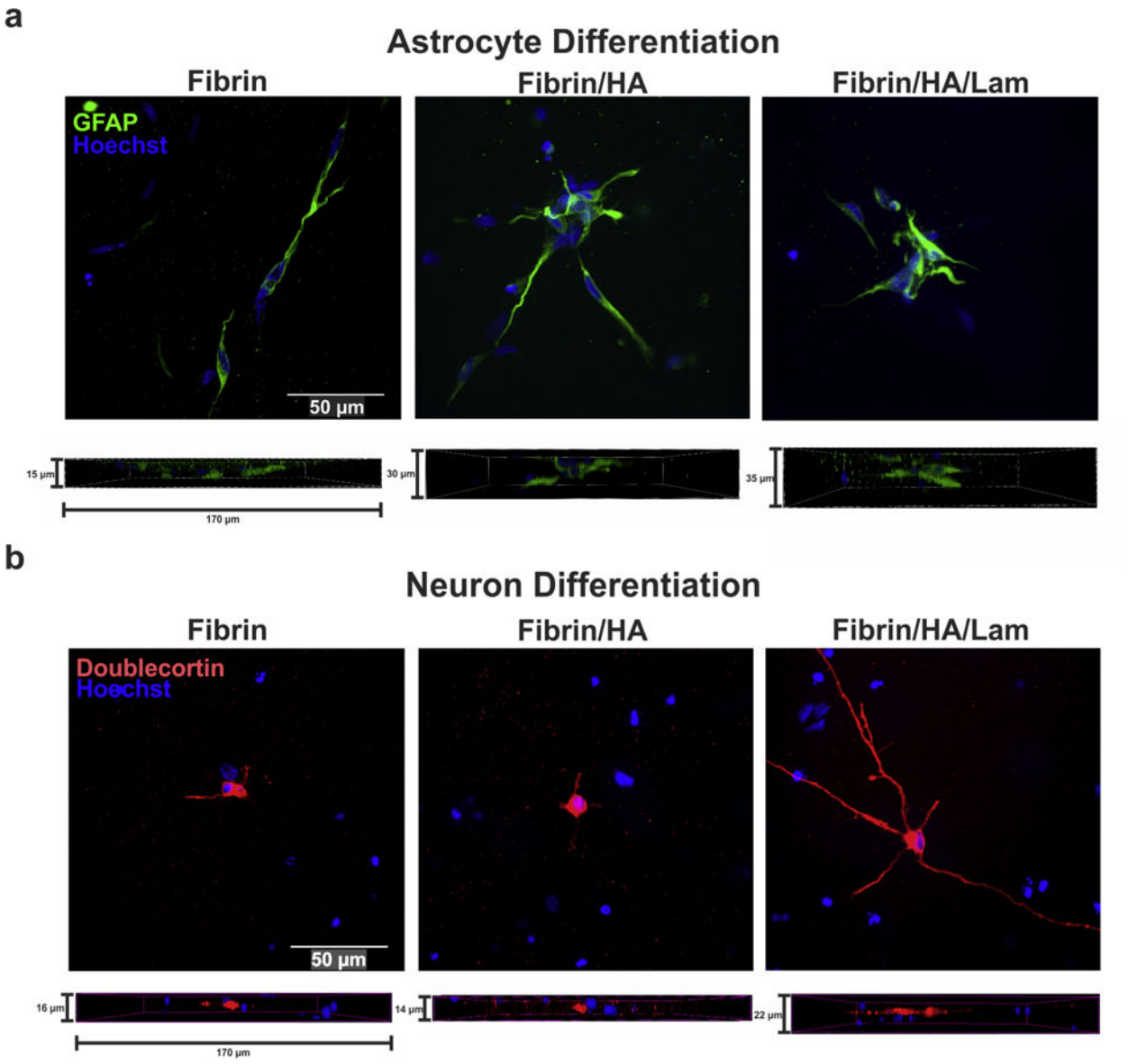

Fig. 5.

HNSPCs differentiate in combination scaffolds. hNSPCs (1×10^5) were differentiated in scaffolds for (a) 5 days to assess astrocytes using the marker GFAP or (b) 14 days for neurons using the marker doublecortin. Lower images in (a) and (b) reveal side view reconstructions to illustrate the three-dimensional nature of the scaffolds and the cell extensions. HNSPCs formed astrocytes and neurons in all scaffolds, but neurite outgrowth was most pronounced in combination scaffolds containing laminin.

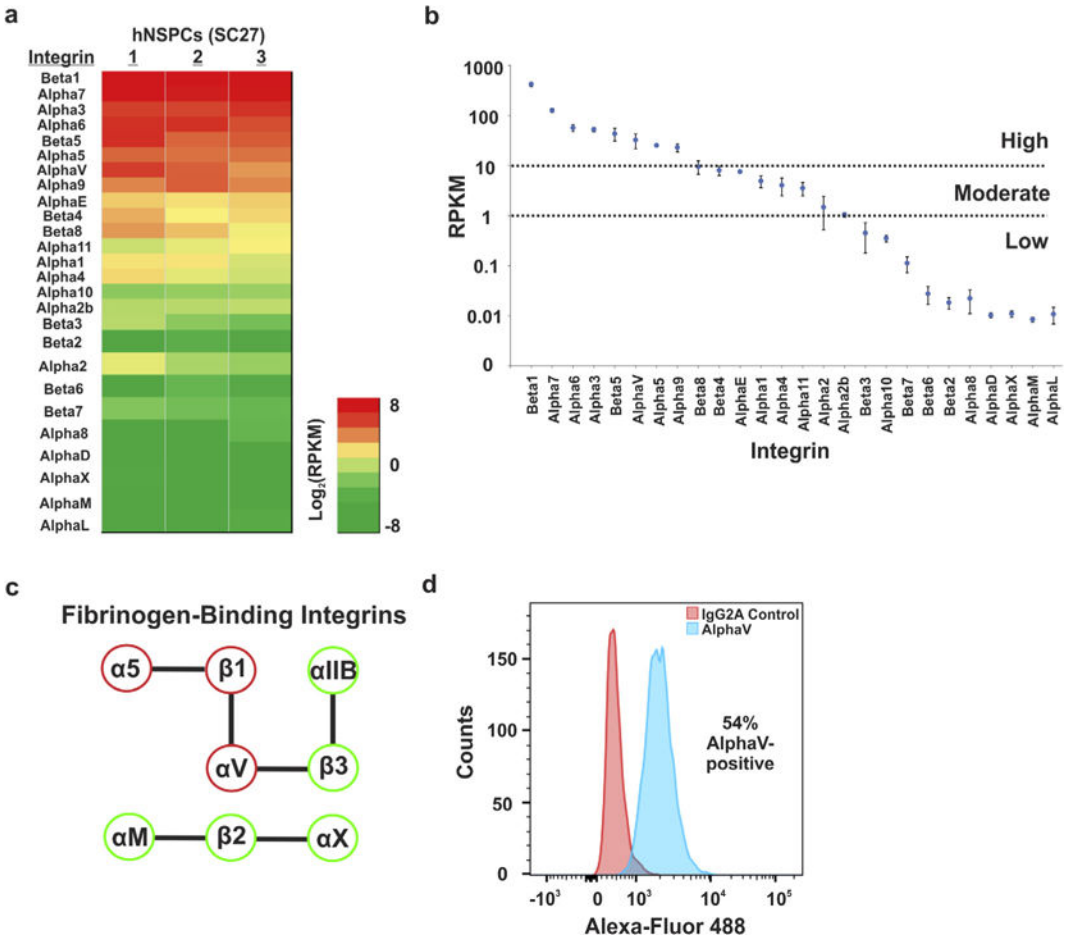

Fig. 6.

HNSPCs express ECM-binding integrins. (a) RNA-seq analysis indicates hNSPC integrin gene expression levels from three biological replicates. Colors indicate the $\log_2$RPKM (reads per kilobase of transcript per million mapped reads) value for each α or β integrin, with red indicating higher expression and green lower expression. (b) The scatterplot displays average RPKM values for each integrin generated from the three replicates of hNSPCs organized from high to low expressers (error is SEM). Genes are clustered into three categories: high (>10 RPKM), moderate (1–10 RPKM), and low (<1 RPKM) expression. Dotted lines indicate 10 RPKM and 1 RPKM boundaries. For comparison, beta-actin, GAPDH, and FGFR1 fall in the highly expressed category, while FGFR2 is moderately expressed, and the muscle marker MyoD shows low to no expression. (c) Integrin binding schematic illustrating α and β integrins identified as fibrinogen-binding heterodimers; lines between α and β pairs indicate heterodimers. Red outlines denote integrins highly expressed by hNSPCs and green indicates lack of expression by hNSPCs [77]. (d) Flow cytometric analysis indicates hNSPC cell surface αV integrin expression. Histogram of Alexa-Fluor 488-positive cells reveals a shift (~54% positive cells) in hNSPCs labeled with an antibody against αV integrin compared to IgG2A isotype control.

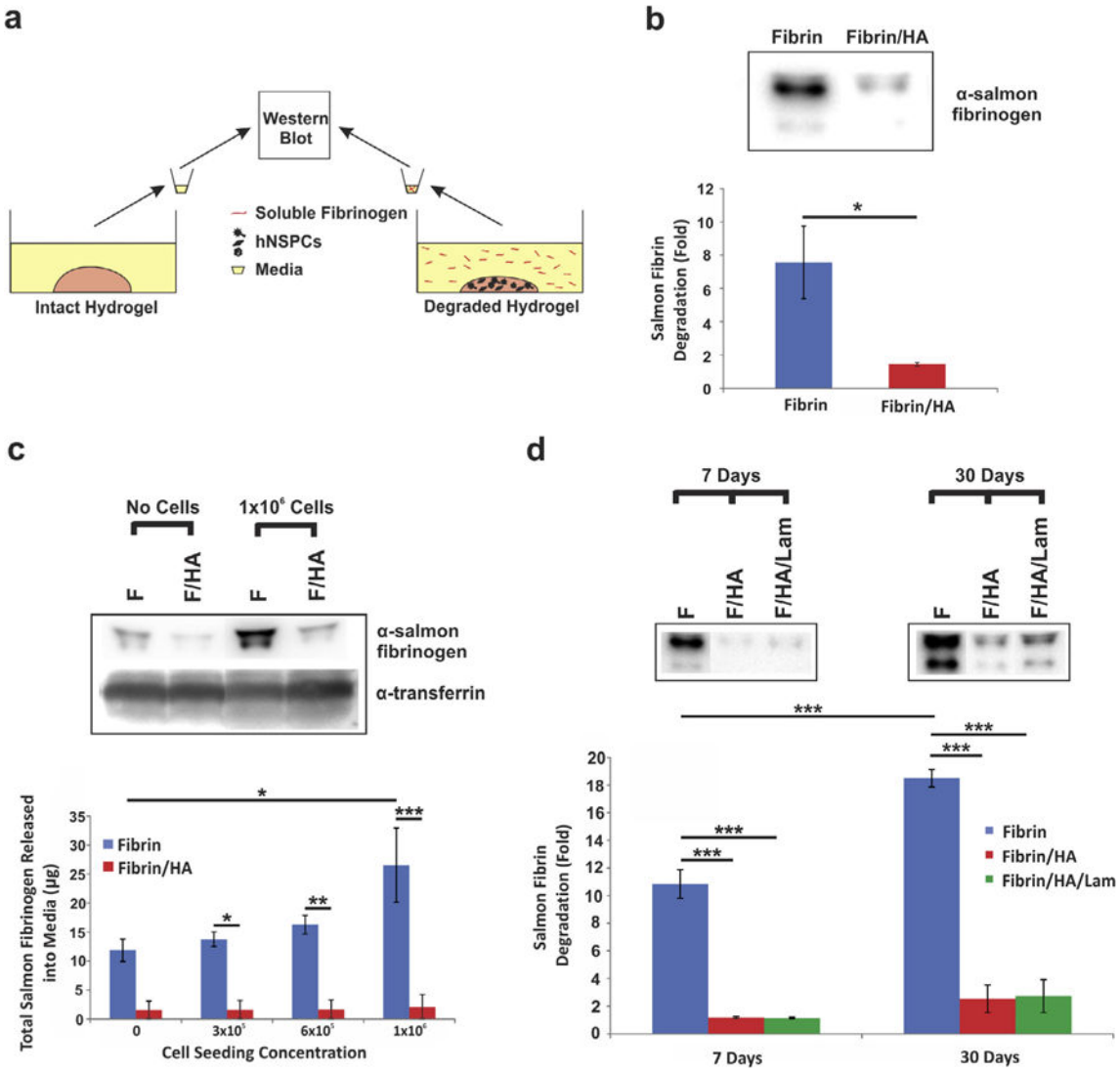

Fig. 7.

Combination scaffolds seeded with hNSPCs degrade more slowly than fibrin scaffolds. (a) HNSPCs were seeded into fibrin only or combination scaffolds with fibrin and HA or fibrin, HA, and laminin and degradation was assessed by measuring release of fibrinogen from the scaffold into the media by Western Blot. Intact hydrogels without cells seeded were used as controls. (b) Fibrinogen released into the media was detected by an anti-salmon fibrinogen antibody [20]. HNSPCs (1×10^5) cause significantly greater degradation of fibrin than combination scaffolds after 7 days in culture. Values are fold change in amount of fibrinogen released into the media relative to that from fibrin/HA hydrogels without seeded cells. P = 0.032. $^*P < 0.05$. (c) Seeding scaffolds with higher numbers of cells (1×10^6) leads to greater release of fibrinogen from fibrin (F) than from fibrin/HA (F/HA) scaffolds after 7 days as detected by Western blot. Transferrin, which is a component of the media, demonstrates approximately equal loading of media per lane. Total fibrinogen released into the media after 7 days increases when scaffolds are seeded with increasing numbers of hNSPC in fibrin scaffolds (blue bars), but is substantially reduced by the presence of HA (red bars). Cells

were seeded at 3×10^5, 6×10^5, and 1×10^6 cells per scaffold. P = 0.027 (fibrin vs. fibrin/HA, 3×10^5), P = 0.007 (fibrin vs. fibrin/HA, 6×10^5), P < 0.0001 (fibrin vs. fibrin/HA, 1×10^6), P = 0.029 (fibrin no cells vs. fibrin 1×10^6). *P < 0.05, **P < 0.01, ***P < 0.001. (d) Degradation induced by hNSPCs (1×10^5) seeded in fibrin scaffolds (F, blue bars) increases with increasing time in culture (7 days vs. 30 days), as shown by fold change in fibrinogen released into the media relative to that from fibrin/HA hydrogels without cells seeded. Fibrin degradation is attenuated drastically by the presence of HA (F/HA, red bars) and HA with laminin (F/HA/Lam, green bars). P = 0.0002 (fibrin 7 days vs. fibrin 30 days), P < 0.0001 (fibrin 7 days vs. fibrin/HA 7 days), P < 0.0001 (fibrin 7 days vs. fibrin/HA/lam 7 days), P < 0.0001 (fibrin 30 days vs. fibrin/HA 30 days), P < 0.0001 (fibrin 30 days vs. fibrin/HA/lam 30 days). ***P < 0.001. Error bars represent SEM. N = 3 independent biological repeats.

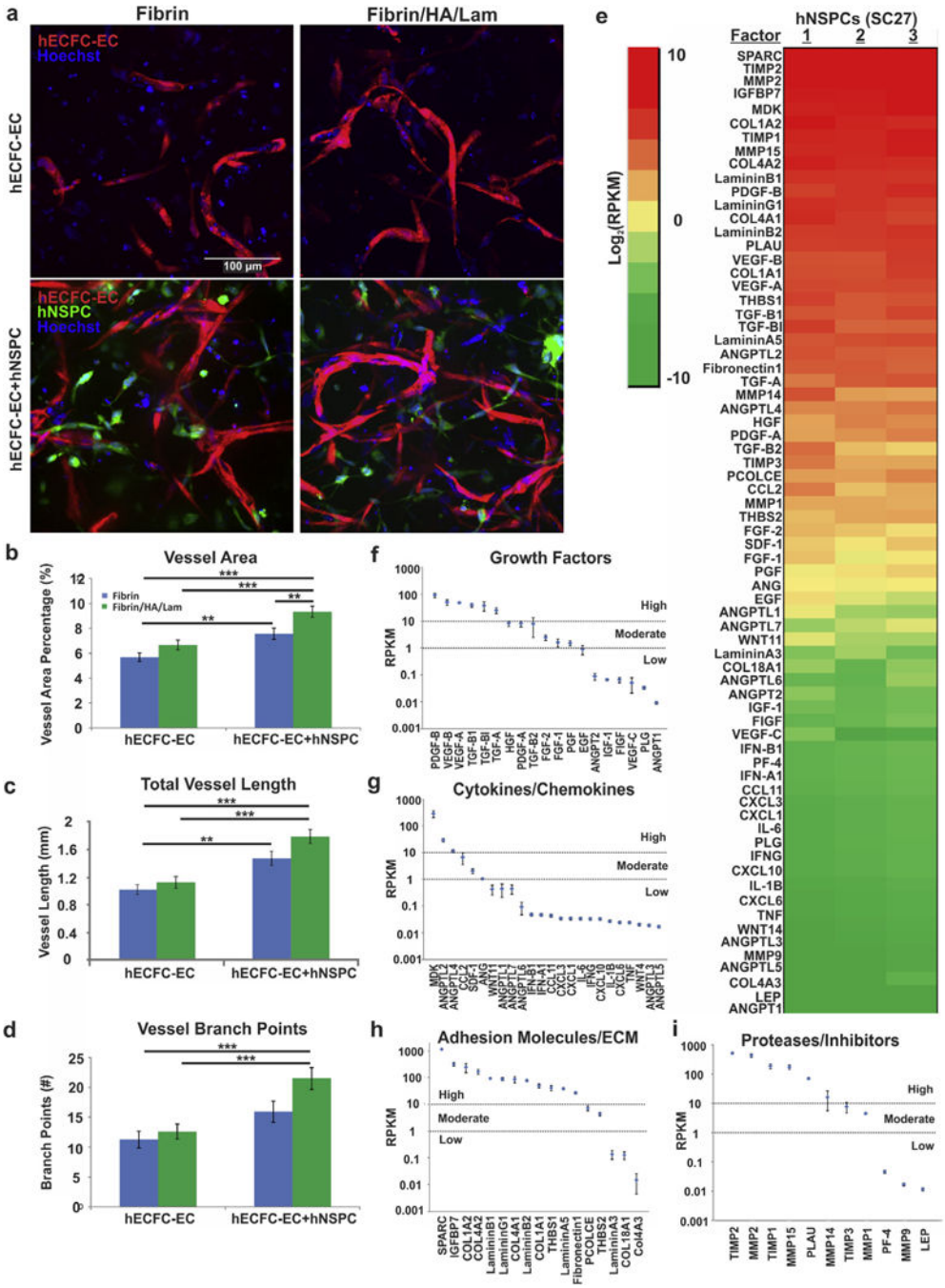

Fig. 8.

Emulation of the human neurovascular niche within scaffolds. (a) HECFC-ECs expressing mCherry were plated at 2.5×10^5 cells per scaffold with or without hNSPCs labeled with Cell Tracker Green at 5×10^4 cells per scaffold. All cell nuclei were detected with Hoechst (blue). Neural and vascular cells interact *in vitro* in the scaffolds and hECFC-ECs form early vessels after 5 days in culture. (b) Quantitative analysis of vessel area indicates a positive effect of hNSPCs on vessel formation with additional increases in vessel formation present in combination scaffolds of fibrin/HA/laminin (green bars) when compared to fibrin

scaffolds (blue bars). P = 1.26E−07 (fibrin/HA/lam − ECFC-EC + NSPC vs. fibrin − ECFC-EC), P = 7.64E−05 (fibrin/HA/lam − ECFC-EC + NSPC vs. fibrin/HA/lam − ECFC-EC), P = 0.0032 (fibrin − ECFC-EC + NSPC vs. fibrin − ECFC-EC), P = 0.0068 (fibrin/HA/lam − ECFC-EC + NSPC vs. fibrin − ECFC-EC + NSPC). (c) Total vessel length is significantly greater in the presence of hNSPCs in both combination and fibrin scaffolds and is highest in combination scaffolds containing both cell types. P = 2.04E−06 (fibrin/HA/lam − ECFC-EC + NSPC vs. fibrin − ECFC-EC), P = 4.97E−05 (fibrin/HA/lam − ECFC-EC + NSPC vs. fibrin/HA/lam − ECFC-EC), P = 0.004 (fibrin − ECFC-EC + NSPC vs. fibrin − ECFC-EC). (d) The number of vessel branch points is significantly enhanced by the presence of hNSPCs and is greatest in combination scaffolds (green bars). P = 1.09E−04 (fibrin/HA/lam − ECFC-EC + NSPC vs. fibrin − ECFC-EC), P = 4.63E−04 (fibrin/HA/lam − ECFC-EC + NSPC vs. fibrin/HA/lam − ECFC-EC). **P < 0.01, ***P < 0.001. Error bars represent SEM. N = 3 independent biological repeats. (e) RNA-seq analysis indicates angiogenic factor gene expression from three biological replicates of hNSPCs. Colors indicate the $\log_2$RPKM value for each factor, with red indicating higher expression and green lower expression (see inset for scale). (f) A scatterplot displays average RPKM values for angiogenic growth factors generated from the three replicates of hNSPCs organized from high to low expressers (error is SEM). Genes are clustered into three categories: high (>10 RPKM), moderate (1–10 RPKM), and low (<1 RPKM) expression. Dotted lines indicate 10 RPKM and 1 RPKM boundaries. For comparison, beta-actin, GAPDH, and FGFR1 fall in the highly expressed category, while FGFR2 is moderately expressed, and the muscle marker MyoD shows low to no expression. (g) Scatterplot of average RPKM values for cytokines and chemokines from the three hNSPC replicates. (h) Scatterplot of average RPKM values for adhesion molecules and ECM from the three hNSPC replicates. (i) Scatterplot of average RPKM values for proteases and inhibitors from the three hNSPC replicates.